

# Augmented coupling interface method for solving eigenvalue problems with sign-changed coefficients

Yu-Chen Shu <sup>a,b,c</sup>, Chiu-Yen Kao <sup>e,f</sup>, I-Liang Chern <sup>c,d,\*</sup>, Chien C. Chang <sup>a,b,c,\*\*</sup>

<sup>a</sup> Division of Mechanics, Research Center for Applied Sciences, Academia Sinica, Taipei 115, Taiwan

<sup>b</sup> Institute of Applied Mechanics, National Taiwan University, Taipei 106, Taiwan

<sup>c</sup> Department of Mathematics and Taida Institute for Mathematical Sciences, National Taiwan University, Taipei 106, Taiwan

<sup>d</sup> National Center for Theoretical Sciences, Math. Division, Taipei Office, Taipei 106, Taiwan

<sup>e</sup> Department of Mathematics, The Ohio State University, OH 43210, USA

<sup>f</sup> Mathematical Biosciences Institute (MBI), The Ohio State University, OH 43210, USA

## ARTICLE INFO

### Article history:

Received 1 December 2009

Received in revised form 5 July 2010

Accepted 1 September 2010

Available online 7 September 2010

### Keywords:

Coupling interface method

Sign-changed coefficients

Eigenvalue problems

## ABSTRACT

In this paper, we propose an augmented coupling interface method on a Cartesian grid for solving eigenvalue problems with sign-changed coefficients. The underlying idea of the method is the correct local construction near the interface which incorporates the jump conditions. The method, which is very easy to implement, is based on finite difference discretization. The main ingredients of the proposed method comprise (i) an adaptive-order strategy of using interpolating polynomials of different orders on different sides of interfaces, which avoids the singularity of the local linear system and enables us to handle complex interfaces; (ii) when the interface condition involves the eigenvalue, the original problem is reduced to a quadratic eigenvalue problem by introducing an auxiliary variable and an interfacial operator on the interface; (iii) the auxiliary variable is discretized uniformly on the interface, the rest of variables are discretized on an underlying rectangular grid, and a proper interpolation between these two grids are designed to reduce the number of stencil points. Several examples are tested to show the robustness and accuracy of the schemes.

© 2010 Elsevier Inc. All rights reserved.

## 1. Introduction

Interface problems attract attention due to their various applications in many different fields, such as fluid dynamics, solid mechanics, electrodynamics, material science, population dynamics, and biochemistry. The interfaces could be material interfaces, phase boundaries, physical boundaries, or others. Theoretically, partial differential equation models invariably involve discontinuities in the physical parameters, coefficients, singular source distribution along interfaces, and non-smooth or even discontinuous solutions. In the cases when the coefficients of elliptic eigenvalue problems are of one sign, many theoretical results and numerical approaches have been proposed. However, in the case when the coefficients change sign across an interface, e.g. population dynamics or dielectric-metal surface plasmonics, the corresponding eigenfunctions may oscillate or decay exponentially (forming a boundary layer) on the two sides of the interfaces. This creates difficulty in numerical computation for such eigenfunctions.

Mathematically, the corresponding equation with sign-changed coefficients changes type, from being elliptic in the normal direction to hyperbolic in the tangential directions of the interface, in order to fit the interface conditions. When this

\* Corresponding author at: Department of Mathematics, National Taiwan University, Taipei 106, Taiwan.

\*\* Corresponding author at: Institute of Applied Mechanics, National Taiwan University, Taipei 106, Taiwan.

E-mail addresses: [scc@math.ntu.edu.tw](mailto:scc@math.ntu.edu.tw) (Y.-C. Shu), [kao@math.ohio-state.edu](mailto:kao@math.ohio-state.edu) (C.-Y. Kao), [chern@math.ntu.edu.tw](mailto:chern@math.ntu.edu.tw) (I-Liang Chern), [mechang@iam.ntu.edu.tw](mailto:mechang@iam.ntu.edu.tw) (C.C.).

equation is solved numerically, the change of type makes the discrete systems non-definite (neither positive-definite nor negative-definite), rendering themselves another difficulty to be resolved numerically. Numerical studies of elliptic interface problems with positive coefficients have a long history. For body-fitting approaches, we refer readers to [1,2]. For finite element approaches, we refer readers to [3–6] and references therein. For finite difference approaches, we refer readers to regularization methods [7,8], the immersed boundary method [9,10], the immersed interface method (IIM) [11–13], a class of methods which are based on dimension-by-dimension approaches [14–18], and the multidimensional piecewise polynomials method [19]. Among these dimension-by-dimension methods, the coupling interface method [18] introduces a coupled equation for the principal second-order derivatives to reduce the number of stencil points, and hence has less restriction on the geometry of the interfaces. But in all of the above methods, the local linear combination of numerical discretization near the interface may not be solvable due to the sign-changed coefficients. The nonexistence of the linear combination is natural when considering problems that have sign-changed coefficients and highly depend on the geometry of the interface. An extremely large linear combination due to the singularity of the coupled equation will have a serious effect on accuracy and condition number.

The present approach resolves the above difficulties by modifying the coupling interface method to solve the eigenvalue problems with sign-changed coefficients. The main ingredients of the proposed method consist of: (i) an adaptive-order strategy on the two sides of the interface which can approach the functions from both sides of the interfaces by polynomials of different orders; (ii) when the interface condition involves the eigenvalue, the introduction of an auxiliary variable and an interfacial operator on the interface reduce the problem to a quadratic eigenvalue problem; (iii) the auxiliary variable is discretized uniformly on the interface, the rest of variables are discretized on an underlying rectangular grid, and a proper interpolation between these two grids are designed to reduce the number of stencil points. In the present study, the method is derived in detail for one- and two-dimensional problems, and can easily be extended to high dimensions, since the discretization procedure is a dimension-by-dimension approach. In each dimension, the unknown function is approximated by polynomials of different orders on each side of the interface and connected by the interface conditions. The orders are changed when the linear combination of the discretization cannot be solved or the interfaces are complex. To stabilize the local inversion, an asymptotic analysis is proposed. To couple information from different dimensions, a coupling equation is solved. This procedure reduces the size of the stencil. The adaptive-order strategy is also used when the coupling equation is not solvable. In addition, this version can integrate with the interfacial operator approach [20] when the interface condition involves the eigenvalue. New unknowns called interfacial variables are introduced and almost uniformly distributed at the interfaces in order to avoid the dependency of the introduced new unknowns. Therefore, the location of the interface condition is realized at the place where the new unknowns are defined, instead of at the intersections of the interface and the underlying rectangular grid lines in the previous work CIM [18]. In the above cases, the methodology is based on the coupling interface method but modifications on derivations of coupling equation and interpolations are needed. We call this version of the coupling interface method the augmented coupling interface method (ACIM). We illustrate our method for two different cases which arise from population dynamics and surface plasmon, in both one and two dimensions. The common point of these two cases is that coefficients change their signs across the interfaces. However, the former is easier than the latter because the jump condition involves the eigenvalue in the latter. In the problem arising from surface plasmon, the jump condition also involves the eigenvalues and it brings another difficulty besides the sign-changed coefficients.

## 2. Eigenvalue problems in population dynamics

In population dynamics, the model

$$-\nabla \cdot (\mathbf{a}\nabla u + \mathbf{b}u) = \lambda mu, \quad \text{in } \Omega \tag{1}$$

was used to describe the stationary dynamics of a population with density  $u = u(\mathbf{r})$  subject to a diffusion matrix  $\mathbf{a} = a_{ij}(\mathbf{r})$ , a drift vector  $\mathbf{b} = b_i(\mathbf{r})$  and a sign indefinite growth rate  $m = m(\mathbf{r})$  where  $\mathbf{r} \in \Omega \subset R^n$ . This model is discussed in detail with different boundary conditions: Dirichlet, Neumann, and Robin type in [21] and the references therein. Cantrell and Cosner [22,23] asked an interesting question: among all functions  $m(\mathbf{r})$  with  $\int_{\Omega} m(\mathbf{r}) = M < 0$  and  $-m_1 < m(\mathbf{r}) < m_2$  ( $m_1, m_2$ , and  $M$  are positive constant), which  $m(x)$  yield the smallest principle eigenvalue  $\lambda_1(m)$ ? From the biological point of view, finding such a minimizing function  $m(\mathbf{r})$  is equivalent to determining the optimal spatial arrangement of the favorable and unfavorable parts of the habitat for species to survive with a fixed amount of resources. The optimal spatial arrangement of  $m(\mathbf{r})$  is found to be of bang-bang type [23–25], i.e.  $m = m_1$  for  $\mathbf{r} \in \Omega^-$  and  $m = m_2$  for  $\mathbf{r} \in \Omega^+$  where  $\overline{\Omega^-} \cup \overline{\Omega^+} = \Omega$ . It is thus important to study this model with sign-changed and discontinuous  $m(\mathbf{r})$  theoretically. This also poses the challenge of developing an accurate and robust numerical algorithm to obtain solutions for Eq. (1).

Suppose the interface  $\Gamma$  is described by a level set function  $\phi(\mathbf{r}) = 0$  which separates the domain  $\Omega$  into two sub domains  $\Omega^- = \{\mathbf{r} | \phi(\mathbf{r}) < 0\}$  and  $\Omega^+ = \{\mathbf{r} | \phi(\mathbf{r}) > 0\}$ . To solve Eq. (1) numerically, a discretization of the left hand side is needed. For the simplicity,  $\mathbf{b}$  is assumed to be zero, and the diffusion matrix  $\mathbf{a}(\mathbf{r})$  and the growth rate  $m(\mathbf{r})$  are assumed to be piecewise constants,

$$\mathbf{a}(\mathbf{r}) = \begin{cases} \mathbf{a}^-\mathbf{I}, & \mathbf{r} \in \Omega^-, \\ \mathbf{a}^+\mathbf{I}, & \mathbf{r} \in \Omega^+, \end{cases} \quad m(\mathbf{r}) = \begin{cases} m^-, & \mathbf{r} \in \Omega^-, \\ m^+, & \mathbf{r} \in \Omega^+, \end{cases} \tag{2}$$

where  $\mathbf{I}$  is an identity matrix. Notice that  $a^\pm$  and  $m^\pm$  may be of different signs in problems with sign-changed coefficients. On the interface, the interface conditions are realized by taking limits of the equation on both sides of the interface

$$[u]_\Gamma = 0, \tag{3}$$

$$[\mathbf{a}\nabla u \cdot \mathbf{n}]_\Gamma = 0, \tag{4}$$

where  $[u]_\Gamma$  stands for the jump of  $u$  across the interface, and  $\mathbf{n}$  represents the outer normal direction of the interface. At the boundary  $\partial\Omega$ , the Robin boundary condition is considered to be

$$u + \gamma \mathbf{a}\nabla u(\mathbf{r}) \cdot \mathbf{n} = 0. \tag{5}$$

Note that the Dirichlet and Neumann boundary conditions are included in the Robin boundary condition by taking  $\gamma = 0$  and  $\infty$ .

**2.1. One-dimensional problems**

In one dimension, assuming that  $\Omega = [0, L]$ , Eq. (1) is reduced to

$$-\frac{1}{m(x)}(a(x)u'(x))' = \lambda u(x), \quad x \in [0, L] \tag{6}$$

and the boundary conditions (5) become

$$u(0) - \gamma(0)a^-(0)u'(0) = 0, \tag{7}$$

$$u(L) + \gamma(L)a^+(L)u'(L) = 0. \tag{8}$$

Without loss of generality, we consider the interface to consist of just one point:  $\Gamma = \{\hat{x}\}$ , where  $0 < \hat{x} < L$ . The jump conditions (3) and (4) are

$$u(\hat{x}^+) - u(\hat{x}^-) := [u]_{\hat{x}} = 0, \tag{9}$$

$$a^+u'(\hat{x}^+) - a^-u'(\hat{x}^-) := [au']_{\hat{x}} = 0, \tag{10}$$

The derivation described below can be easily extended to a more general interface that consists of more points.

We use the standard central finite difference discretization for stencils which are away from the interface. For the grid points near the interface, i.e., where the stencils of the standard finite difference discretization are not in the same region, local construction from one-sided grid values is used. Here we lay out the details. Let  $h = L/N$ ,  $x_i = ih$ ,  $0 \leq i \leq N$ . Suppose the interface point  $\hat{x} = x_i + \alpha h$  is located in the interval  $[x_i, x_{i+1})$ . Let  $\beta = 1 - \alpha$ . Local polynomials of degree  $p$  and  $q$  are used to approximate  $u$  on the two sides of  $\hat{x}$ . The grid values  $u_j$ ,  $i - p + 1 \leq j \leq i + q$ , are used to reconstruct the local one-side Newton polynomials,

$$u(x) = \begin{cases} \sum_{\ell=0}^{p-1} \left( [u_i, u_{i-1}, \dots, u_{i-\ell}] \prod_{j=0}^{\ell-1} (x - x_{i-j}) \right) + c_1 \prod_{j=0}^{p-1} (x - x_{i-j}), & x < \hat{x}; \\ \sum_{\ell=1}^q \left( [u_{i+1}, u_{i+2}, \dots, u_{i+\ell}] \prod_{j=1}^{\ell-1} (x - x_{i+j}) \right) + c_2 \prod_{j=1}^q (x - x_{i+j}), & x > \hat{x}, \end{cases} \tag{11}$$

where  $[u_i, u_{i-1}, \dots, u_{i-\ell}]$  and  $[u_{i+1}, u_{i+2}, \dots, u_{i+\ell}]$  are Newton's divided differences. The coefficients  $c_1$  and  $c_2$  are determined by substituting Eq. (11) into the two jump conditions Eqs. (9) and (10) which result in a  $2 \times 2$  linear equations for  $c_1$  and  $c_2$ . The determinant  $D_{p,q}$  of this linear system is listed in Table 1 for various  $p$  and  $q$ . When  $a$  is always positive, the uniqueness is guaranteed [18]. However, if  $a$  has different signs on the two sides of the interface, this determinant may be zero. Fortunately, for sign-changed problems, the non-existence of  $c_1$  and  $c_2$  happens at different  $\alpha$ 's when  $p$  and  $q$  vary. We can alter the order  $p$  and  $q$  to avoid occurrence of zero determinant.

**Table 1**

The determinant of the linear system for solving  $c_1$  and  $c_2$  when two polynomials of degree  $p$  and  $q$  are used to approximate  $u$  on the left (minus) and right (plus) side of the interface, respectively. Here, a uniform mesh with mesh size  $h$  is applied. The interface is located at  $\hat{x} = x_i + \alpha h$  for some  $i$  and  $\beta = 1 - \alpha$ . The symbols  $a^-$  and  $a^+$  are the coefficients on the left ( $-$ ) and right ( $+$ ) side of the interface.

$p$	$q$	The determinant $D_{p,q}$ of the linear system for solving $c_1$ and $c_2$
1	1	$a^- \beta + a^+ \alpha$
2	1	$a^- \beta(1 + 2\alpha) + a^+ \alpha(1 + \alpha)$
1	2	$a^- \beta(1 + \beta) + a^+ \alpha(1 + 2\beta)$
2	2	$a^- \beta(1 + \beta)(1 + 2\alpha) + a^+ \alpha(1 + \alpha)(1 + 2\beta)$
3	2	$a^- \beta(1 + \beta)(3\alpha^2 + 6\alpha + 2) + a^+ \alpha(1 + \alpha)(2 + \alpha)(1 + 2\beta)$
2	3	$a^- \beta(1 + \beta)(2 + \beta)(1 + 2\alpha) + a^+ \alpha(1 + \alpha)(3\beta^2 + 6\beta + 2)$

Let us determine the orders we should choose on different sides of the interface to avoid the singularity of the local linear system. We introduce a normalized determinant  $f_{p,q}(\alpha, \rho) = D_{p,q}/a^-$ , where  $\rho = a^+/a^-$  and we assumed that  $|a^-| \leq |a^+|$  without loss of generality. Let  $\alpha_{p,q}(\rho)$  be the solution of  $f_{p,q}(\alpha_{p,q}(\rho), \rho) = 0$ . We claim that both  $f_{p+1,q}(\alpha_{p,q}(\rho), \rho) \neq 0$  and  $f_{p,q+1}(\alpha_{p,q}(\rho), \rho) \neq 0$ . Below, we prove this claim for  $p = q = 2$ . First, the relation of  $\rho$  and  $\alpha_{2,2}$  is

$$\rho = -\frac{(1 - \alpha_{2,2})(2 - \alpha_{2,2})(1 + 2\alpha_{2,2})}{\alpha_{2,2}(1 + \alpha_{2,2})(3 - 2\alpha_{2,2})}. \tag{12}$$

By substituting (12) in  $f_{3,2}(\alpha_{2,2}(\rho), \rho)$  and  $f_{2,3}(\alpha_{2,2}(\rho), \rho)$ , we arrive at

$$f_{3,2}(\alpha_{2,2}(\rho), \rho) = \alpha_{2,2}(\rho)(1 - \alpha_{2,2}(\rho))(2 - \alpha_{2,2}(\rho))(1 + \alpha_{2,2}(\rho)) \neq 0, \tag{13}$$

$$f_{2,3}(\alpha_{2,2}(\rho), \rho) = -\frac{(1 - \alpha_{2,2}(\rho))^2(2 - \alpha_{2,2}(\rho))^2(1 + 2\alpha_{2,2}(\rho))}{(3 - 2\alpha_{2,2}(\rho))} \neq 0, \tag{14}$$

since  $0 < \alpha_{2,2}(\rho) < 1$ . Fig. 1 shows the values of  $f_{3,2}(\alpha_{2,2}(\rho), \rho)$  and  $f_{2,3}(\alpha_{2,2}(\rho), \rho)$  when  $\rho$  varies from  $-20$  to  $-1$ . Moreover, we look for the asymptotic behaviors of  $f_{3,2}$  and  $f_{2,3}$ . It follows from Eq. (12). For  $\rho \ll -1$  and  $0 < \alpha_{2,2} < 1$ , we

$$\alpha_{2,2}(\rho) \approx -\frac{2}{3}\rho^{-1}. \tag{15}$$

By applying (15), the asymptotic behaviors of these two functions are

$$f_{3,2}(\alpha_{2,2}(\rho), \rho) \approx -\frac{4}{3}\rho^{-1}, \quad f_{2,3}(\alpha_{2,2}(\rho), \rho) \approx -\frac{4}{3}, \quad \text{for } \rho \ll -1. \tag{16}$$

The analysis above indicates that we should use higher order approximation in the region with a larger absolute value of  $a$  in order to get a stable solution. This motivates us to define the following adaptive-order strategy:

1. First, choose the orders  $p$  and  $q$  to approximate  $u$  on different sides of the interface.
2. If  $f_{p,q}(\alpha, \rho)$  is smaller than a prescribed tolerance, then the order in the region with a larger absolute value of  $a$  is increased by 1.

A generalized pseudo code is given in the Appendix A.

Once we have the local approximated polynomial with  $p, q \geq 2$ , we can approximate  $u''(x_i)$  by differentiating this local polynomial twice to get the following approximation:

$$u''(x_i) = \frac{1}{h^2} \mathcal{L}(u_{i-p+1:i+q}, [u]_{i_x}, [au']_{i_x}) + O(h^{\min\{p,q\}-1}), \tag{17}$$

where the operator  $\mathcal{L}$  is a linear combination of grid values  $u_{i-p+1:i+q}$  and the jump conditions  $([u]_{i_x}$  and  $[au']_{i_x})$ . For example, when  $p = q = 2$ ,

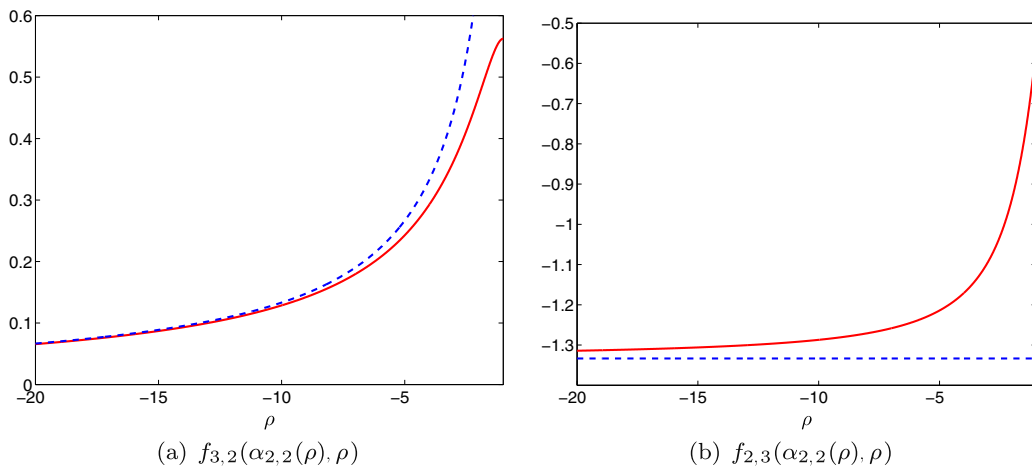


Fig. 1. The values of  $f_{3,2}(\alpha_{2,2}(\rho), \rho)$  and  $f_{2,3}(\alpha_{2,2}(\rho), \rho)$  when  $\rho$  varies from  $-20$  to  $-1$ . The blue dashed lines are the asymptotic behavior computed from Eq. (16). (For interpretation of the references to colour in this figure legend, the reader is referred to the web version of this article.).

$$\mathcal{L}(u_{i-p+1:i+q}, [u]_{\bar{x}}, [au']_{\bar{x}}) = \frac{1}{D_{2,2}} \begin{bmatrix} (\beta + \beta)^2 a^- + \alpha(1 + 2\beta)a^+ \\ -(\beta + \beta^2)a^- - (1 + \alpha)(1 + 2\beta)a^+ \\ (1 + \beta)^2 a^+ \\ -\beta^2 a^+ \\ -(1 + 2\beta)a^+ \\ -(\beta + \beta^2)h \end{bmatrix}^T \begin{bmatrix} u_{i-1} \\ u_i \\ u_{i+1} \\ u_{i+2} \\ [u]_{\bar{x}} \\ [au']_{\bar{x}} \end{bmatrix}. \tag{18}$$

In some cases, we may also use lower-order approximation. If  $p = 1$ , we can only approximate  $u'(x_{i+1/2})$  in  $\Omega^-$  by differentiating the local polynomial once:

$$u'(x_{i+1/2}) \approx \frac{1}{h} \mathcal{D}(u_{i:i+q}, [u]_{\bar{x}}, [au']_{\bar{x}}), \tag{19}$$

where the operator  $\mathcal{D}$  is a linear combination of grid values  $u_{i:i+q}$  and the jump conditions  $([u]_{\bar{x}}$  and  $[au']_{\bar{x}})$ . For example, when  $p = 1$  and  $q = 2$ ,

$$\mathcal{D}(u_{i-p+1:i+q}, [u]_{\bar{x}}, [au']_{\bar{x}}) = \frac{1}{D_{1,2}} \begin{bmatrix} -(1 + 2\beta)a^+ \\ (1 + \beta)^2 a^+ \\ -\beta^2 a^+ \\ -(1 + 2\beta)a^+ \\ -(\beta + \beta^2)h \end{bmatrix}^T \begin{bmatrix} u_i \\ u_{i+1} \\ u_{i+2} \\ [u]_{\bar{x}} \\ [au']_{\bar{x}} \end{bmatrix}. \tag{20}$$

And the second order derivative  $u''(x_i)$  is approximated by

$$u''(x_i) \approx \frac{1}{h} (u'(x_{i+1/2}) - u'(x_{i-1/2})),$$

where  $u'(x_{i-1/2})$  is approximated by the standard central finite difference method since  $x_{i-1}$  and  $x_i$  are in the same domain.

Notice that the jump conditions  $[u]_{\bar{x}}$  and  $[au']_{\bar{x}}$  are trivial in one dimension, we can omit these two terms in one dimension. However, they are not trivial in higher dimensions, especially when the normal vectors are not parallel to the coordinate direction. Therefore, we use the general forms in one dimension. The coefficient of  $[au']_{\bar{x}}$  listed in Table 2 will be used in the derivations in two dimensions. In addition, this study is an augmented version of the coupling interface method partly because we allow the orders of interpolations on different sides of the interfaces may be different. The cases  $p = q = 1$  and  $p = q = 2$  correspond respectively to the first order version (CIM1,  $p = q = 1$ ) and the second order version (CIM2,  $p = q = 2$ ) of the coupling interface method [18] in one dimension.

2.2. Two-dimensional problems

In two-dimensional problems, the eigenvalue problem (1) is reduced to

$$-\frac{1}{m(x,y)} \nabla_2 \cdot (a(x,y) \nabla_2 u(x,y)) = \lambda u(x,y), \quad x \in \Omega, \tag{21}$$

where  $\nabla_2 = (\partial/\partial x, \partial/\partial y)$ . We drop the subindex of  $\nabla_2$  in the later derivation for simplicity. Suppose that domain  $\Omega = [0,L] \times [0,L]$  is a square and a uniform grid  $(x_i, y_j) = (ih, jh)$  is adopted, where  $h = L/N$ . The notation  $u_{i_1:i_2, j_1:j_2}$  means all the grid values  $u_{i,j}$ ,  $i_1 \leq i \leq i_2, j_1 \leq j \leq j_2$ . Standard finite difference discretization is used for stencils which are away from the interface. At a point near the interface, i.e., where the stencils of the standard finite difference discretization are not in the same region, a dimension-by-dimension approach is used. Without loss of generality, suppose that  $(x_i, y_j)$  is a point near the interface and lies in  $\Omega^-$ . The abbreviation  $u_{ij} = u(x_i, y_j)$  is used for simplicity. A grid segment is a segment which connects two nearest grid points. Here we first consider two different cases of intersection which occur most often:  $\Gamma$  intersects either one grid segment (see Fig. 2(a)) or two grid segments in different directions, see Fig. 2(b). In these two cases, ACIM2 is adoptable. Here we have assumed that the mesh size is fine enough to resolve the geometry of the interfaces and there is at most one intersection in one grid segment. This is valid when the mesh size is very fine. If the mesh is not very fine, there may be more than one intersection in a grid segment. In this situation, we use the following criteria:

Table 2

The coefficients of  $[au']_{\bar{x}}$  in the derivation when  $p$  and  $q$  vary. When  $p = 1$  or  $q = 1$ , the coefficient is used in  $\mathcal{D}$ . When  $p, q \geq 2$ , the coefficient is used in  $\mathcal{L}$ . Here we assume that  $h = 1$ . Scaling for  $h \neq 1$  is required.

$(p, q)$	(1,1)	(2,1)	(1,2)	(2,2)	(3,2)	(2,3)
Coefficient	$-\frac{\beta}{D_{1,1}}$	$-\frac{\beta}{D_{2,1}}$	$-\frac{\beta(\beta+1)}{D_{1,2}}$	$-\frac{\beta(\beta+1)}{D_{2,2}}$	$-\frac{\beta(\beta+1)}{D_{2,3}}$	$-\frac{2\beta(\beta+1)(\beta+2)}{D_{2,3}}$

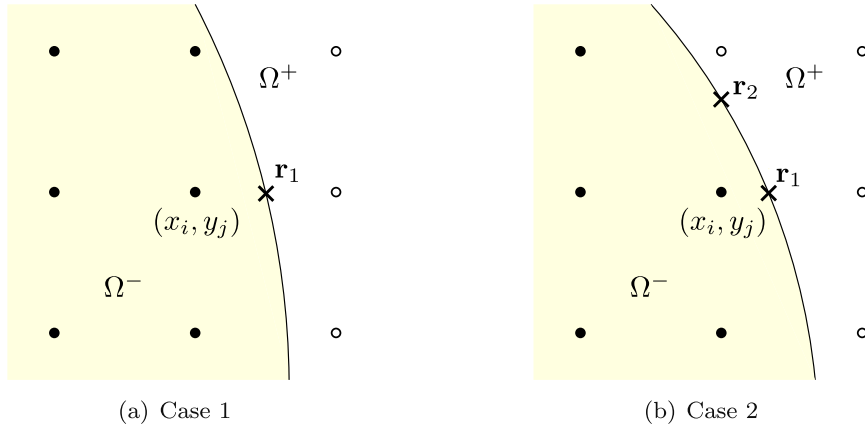


**Fig. 2.** Intersection of interface and the grid segments. Case 1: the interface intersects the grid segment in the  $x$ -direction only. Case 2: the interface intersects grid segments in both  $x$ - and  $y$ -directions. The regions colored by light yellow and white are  $\Omega^-$  and  $\Omega^+$ , respectively. The disks and circles are the grid points in  $\Omega^-$  and  $\Omega^+$ , respectively. (For interpretation of the references to colour in this figure legend, the reader is referred to the web version of this article.)

- If the two ends of the grid segment are not in the same domain, we can choose any one of the intersections in the following derivation if there is more than one intersection.
- If the two ends of the grid segment are in the same domain, no special treatment is needed even if there are intersections in the grid segment.

In addition, this situation will occur when the interface is complicated. The issue of complex interfaces will be discussed later in this section.

*The interface intersects the grid segment in the  $x$ -direction only* Suppose that the intersection of the interface and the grid line is lying in  $[x_i, x_{i+1}) \times \{y_j\}$  (we label the intersection as  $\mathbf{r}_1 = (x_i + \alpha_1 h, y_j)$ ). In this case, the following terms can be approximated by the nearby points

$$\frac{\partial^2 u_{ij}}{\partial y^2} = \frac{u_{i,j+1} - 2u_{ij} + u_{i,j-1}}{h^2} + O(h^2), \tag{22}$$

$$\frac{\partial^2 u_{ij}}{\partial x \partial y} = \frac{u_{i,j+1} - u_{i,j-1} - u_{i-1,j+1} + u_{i-1,j-1}}{2h^2} + O(h). \tag{23}$$

Our goal is to derive a first-order finite difference approximation for  $\frac{\partial^2 u_{ij}}{\partial x^2}$ . The one-dimensional approach of  $\frac{\partial^2 u_{ij}}{\partial x^2}$  is derived by using the jump conditions (3) and an artificial jump  $[a \frac{\partial u}{\partial x}]_{\mathbf{r}_1}$ :

$$\frac{\partial^2 u_{ij}}{\partial x^2} \approx \frac{1}{h^2} \mathcal{L}_x(u_{i-p_1+1:i+q_1,j}) + \frac{\sigma_1}{h} \left[ a \frac{\partial u}{\partial x} \right]_{\mathbf{r}_1}, \tag{24}$$

where  $\mathcal{L}_x$  is a linear combination derived from the one-dimensional problem;  $p_1$  and  $q_1$  are the adaptive orders (the adaptive-order strategy is used) of the local polynomials. The coefficient  $\sigma_1$  of the jump data are explicitly written for the following derivation. The formula of  $\sigma_1$  is listed in Table 2 when  $p_1$  or  $q_1$  is less than 3. By using the jump conditions  $[u]_{\mathbf{r}_1} = 0$  and  $[a \nabla u \cdot \mathbf{n}_1]_{\mathbf{r}_1} = 0$ , the decomposition of the jump data is derived:

$$\left[ a \frac{\partial u}{\partial x} \right]_{\mathbf{r}_1} := a^+ \frac{\partial u}{\partial x}(\mathbf{r}_1^+) - a^- \frac{\partial u}{\partial x}(\mathbf{r}_1^-) = ([a] \mathbf{t}_1 \cdot \mathbf{e}_1) \nabla u(\mathbf{r}_1^-) \cdot \mathbf{t}_1 \tag{25}$$

where  $[a] = a^+ - a^-$ ;  $\mathbf{e}_1 = (1, 0)$  is the Euclidean unit vector;  $\mathbf{n}_1$  is the unit outer normal vector at the interface point  $\mathbf{r}_1$ ;  $\mathbf{t}_1 = (\mathbf{e}_1 - (\mathbf{e}_1 \cdot \mathbf{n}_1) \mathbf{n}_1) / (\|\mathbf{e}_1 - (\mathbf{e}_1 \cdot \mathbf{n}_1) \mathbf{n}_1\|)$  is the computed unit tangential vector at  $\mathbf{r}_1$ . Notice that when the interface is a vertical straight line, i.e.  $\mathbf{n}_1 = \mathbf{e}_1$ , we would set  $\mathbf{t}_1 = \mathbf{e}_2$  and get  $\mathbf{t}_1 \cdot \mathbf{e}_1 = 0$ . The jump  $[a \frac{\partial u}{\partial x}]_{\mathbf{r}_1}$  would be identical to  $[a \nabla u \cdot \mathbf{n}]_{\mathbf{r}_1}$ , which is zero due to the jump condition (4). For the sake of reducing the stencil, only the order of truncation error is the main concern. Therefore, the gradient in Eq. (25) is approximated by

$$\nabla u(\mathbf{r}_1^-) = \left[ \frac{1}{h} (u_{ij} - u_{i-1,j}) + \left(\frac{1}{2} + \alpha_1\right) h \frac{\partial^2 u_{ij}}{\partial x^2} \right] + O(h^2). \tag{26}$$

By combining Eqs. (23)–(26), we arrive at

$$\left(1 - \left(\frac{1}{2} + \alpha_1\right)\sigma_1[a](\mathbf{t}_1 \cdot \mathbf{e}_1)^2\right) \frac{\partial^2 u_{ij}}{\partial x^2} = \frac{1}{h^2} (\mathcal{L}_x(u_{i-p_1+1:i+q_1j}) + \mathcal{T}_x(u_{i-1:i,j-1:j+1})) + O(h), \tag{27}$$

where  $\mathcal{T}_x$  is a linear combination which collects the approximation in the gradient term,

$$\mathcal{T}_x(u_{i-1:i,j-1:j+1}) = \sigma_1[a]\mathbf{t}_1 \cdot \mathbf{e}_1 \left[ \frac{u_{ij} - u_{i-1j}}{\frac{1}{2}((1 + \alpha_1)(u_{ij+1} - u_{ij-1}) - \alpha_1(u_{i-1j+1} - u_{i-1j-1}))} \right] \cdot \mathbf{t}_1. \tag{28}$$

The left hand side of Eq. (27) may be zero with the sign-changed coefficients. If the left hand side is smaller than the tolerance, the order in the region with a large absolute value of  $a$  will be increased by 1. In other words, if  $|a^-| \geq |a^+|$ , then  $p_1$  is increased by 1. Otherwise  $q_1$  is increased by 1. By combining (22) and (23), the discretization of (21) is obtained.

On the other hand, if the interface intersects grid segments in the  $y$ -direction only, the derivation is the same by simply exchanging  $x$  and  $y$ ,  $\mathbf{e}_1$  and  $\mathbf{e}_2$  due to the  $x$ - $y$  symmetry.

*The interface intersects grid segments in both  $x$ - and  $y$ -directions* Suppose that the intersections of the interface and the grid line are lying in  $[x_i, x_{i+1}] \times [y_j]$  (we label the intersection as  $\mathbf{r}_1 = (x_i + \alpha_1 h, y_j)$ ) and  $[x_i] \times [y_j, y_{j+1}]$  (we label it as  $\mathbf{r}_2 = (x_i, y_j + \alpha_2 h)$ ). In this case, only the cross derivative terms can be approximated by the nearby points

$$\frac{\partial^2 u_{ij}}{\partial x \partial y} = \frac{u_{ij} - u_{ij-1} - u_{i-1j} + u_{i-1j-1}}{h^2} + O(h). \tag{29}$$

A dimension-by-dimension approach in the  $x$ - and  $y$ -directions is applied by using jump condition (3) and two artificial jump conditions  $[a \frac{\partial u}{\partial x}]_{\mathbf{r}_1}$  and  $[a \frac{\partial u}{\partial y}]_{\mathbf{r}_2}$ :

$$\frac{\partial^2 u_{ij}}{\partial x^2} \approx \frac{1}{h^2} \mathcal{L}_x(u_{i-p_1+1:i+q_1j}) + \frac{\sigma_1}{h} \left[ a \frac{\partial u}{\partial x} \right]_{\mathbf{r}_1}, \tag{30}$$

$$\frac{\partial^2 u_{ij}}{\partial y^2} \approx \frac{1}{h^2} \mathcal{L}_y(u_{ij-p_2+1:j+q_2}) + \frac{\sigma_2}{h} \left[ a \frac{\partial u}{\partial y} \right]_{\mathbf{r}_2}, \tag{31}$$

where the coefficients  $\sigma_1$  and  $\sigma_2$  of the jump data are explicitly written for the following derivation;  $(p_1, q_1)$  and  $(p_2, q_2)$  are the adaptive orders of the local polynomials in the  $x$ - and  $y$ -directions, respectively. The decomposition of the jump data is similar to the previous case:

$$\left[ a \frac{\partial u}{\partial x} \right]_{\mathbf{r}_1} := a^+ \frac{\partial u}{\partial x}(\mathbf{r}_1^+) - a^- \frac{\partial u}{\partial x}(\mathbf{r}_1^-) = ([a]\mathbf{t}_1 \cdot \mathbf{e}_1) \nabla u(\mathbf{r}_1^-) \cdot \mathbf{t}_1, \tag{32}$$

$$\left[ a \frac{\partial u}{\partial y} \right]_{\mathbf{r}_2} := a^+ \frac{\partial u}{\partial y}(\mathbf{r}_2^+) - a^- \frac{\partial u}{\partial y}(\mathbf{r}_2^-) = ([a]\mathbf{t}_2 \cdot \mathbf{e}_2) \nabla u(\mathbf{r}_2^-) \cdot \mathbf{t}_2, \tag{33}$$

where  $\mathbf{e}_1 = (1, 0)$  and  $\mathbf{e}_2 = (0, 1)$  are the Euclidean unit vectors;  $\mathbf{n}_1$  and  $\mathbf{n}_2$  are the unit outer normal vectors at the interface point  $\mathbf{r}_1$  and  $\mathbf{r}_2$ , respectively;  $\mathbf{t}_1 = (\mathbf{e}_1 - (\mathbf{e}_1 \cdot \mathbf{n}_1)\mathbf{n}_1) / (\|\mathbf{e}_1 - (\mathbf{e}_1 \cdot \mathbf{n}_1)\mathbf{n}_1\|)$  and  $\mathbf{t}_2 = (\mathbf{e}_2 - (\mathbf{e}_2 \cdot \mathbf{n}_2)\mathbf{n}_2) / (\|\mathbf{e}_2 - (\mathbf{e}_2 \cdot \mathbf{n}_2)\mathbf{n}_2\|)$  are the computed unit tangential vectors at  $\mathbf{r}_1$  and  $\mathbf{r}_2$ , respectively. The gradient terms in Eqs. (32) and (33) are approximated by

$$\nabla u(\mathbf{r}_1^-) = \left[ \frac{1}{h}(u_{ij} - u_{i-1j}) + \left(\frac{1}{2} + \alpha_1\right)h \frac{\partial^2 u_{ij}}{\partial x^2} \right] + O(h^2), \tag{34}$$

$$\nabla u(\mathbf{r}_2^-) = \left[ \frac{1}{h}(u_{ij} - u_{i-1j}) + \frac{1}{2}h \frac{\partial^2 u_{ij}}{\partial x^2} + \alpha_2 h \frac{\partial^2 u_{ij}}{\partial x \partial y} \right] + O(h^2). \tag{35}$$

By combining Eqs. (29)–(35), we arrive at a couple equation:

$$\mathbf{M} \begin{bmatrix} \frac{\partial^2 u_{ij}}{\partial x^2} \\ \frac{\partial^2 u_{ij}}{\partial y^2} \end{bmatrix} = \frac{1}{h^2} \begin{bmatrix} \mathcal{L}_x(u_{i-p_1+1:i+q_1j}) + \mathcal{T}_x(u_{i-1:i,j-1:j+1}) \\ \mathcal{L}_y(u_{ij-p_2+1:j+q_2}) + \mathcal{T}_y(u_{i-1:i,j-1:j+1}) \end{bmatrix}, \tag{36}$$

where

$$\mathbf{M} = \begin{bmatrix} 1 - \left(\frac{1}{2} + \alpha_1\right)\sigma_1[a](\mathbf{t}_1 \cdot \mathbf{e}_1)^2 & -\frac{1}{2}\sigma_1[a](\mathbf{t}_1 \cdot \mathbf{e}_1)(\mathbf{t}_1 \cdot \mathbf{e}_2) \\ -\frac{1}{2}\sigma_2[a](\mathbf{t}_2 \cdot \mathbf{e}_1)(\mathbf{t}_2 \cdot \mathbf{e}_2) & 1 - \left(\frac{1}{2} + \alpha_2\right)\sigma_2[a](\mathbf{t}_2 \cdot \mathbf{e}_2)^2 \end{bmatrix} \tag{37}$$

and the linear combinations  $\mathcal{T}_x$  and  $\mathcal{T}_y$  are

$$\mathcal{T}_x(u_{i-1:i,j-1:j+1}) = \sigma_1[a](\mathbf{t}_1 \cdot \mathbf{e}_1) \left[ \frac{u_{ij} - u_{i-1j}}{(1 + \alpha_1)(u_{ij} - u_{ij-1}) - \alpha_1(u_{i-1j} - u_{i-1j-1})} \right] \cdot \mathbf{t}_1, \tag{38}$$

$$\mathcal{T}_y(u_{i-1:i,j-1:j}) = \sigma_2[a](\mathbf{t}_2 \cdot \mathbf{e}_2) \begin{bmatrix} (1 + \alpha_1)(u_{ij} - u_{i-1,j}) - \alpha_1(u_{ij-1} - u_{i-1,j-1}) \\ u_{ij} - u_{ij-1} \end{bmatrix} \cdot \mathbf{t}_2. \tag{39}$$

The determinant of  $\mathbf{M}$  may be zero when considering the problem with the sign-changed coefficients.

If it is smaller than the tolerance, the order in the region with a large absolute value of  $a$  will increase by 1. The details of altering  $p_{1:2}$  and  $q_{1:2}$  are given when we discuss the adaptive-order strategy for complex interfaces.

It is noted that a high order approximation can be achieved by similar derivations. For example, when  $p_1, q_1, p_2$  and  $q_2$  are greater than 4, a fourth order approximation of Eq. (21) can be derived. But the approximation of the gradient at the interface and the cross term is more complicated and highly depends on the geometry of the interface. We omit the derivation of the higher order scheme here.

### 2.3. The adaptive-order strategy for complex interfaces in two dimensions

For complex interfaces, how to choose the grid points is the main concern. For example, in Fig. 2, if the grid points  $(x_{i-1:i}, y_j)$ ,  $(x_i, y_{j-2:j})$  and  $(x_{i-1}, y_{j-1})$  are in the domain  $\Omega^-$  and the grid points  $(x_{i+1:i+2}, y_j)$  and  $(x_i, y_{j+1:j+2})$  are in the domain  $\Omega^+$ , this adaptive-order strategy is said to be feasible at the grid point  $(x_i, y_j)$  for the orders  $(p_1, q_1) = (2, 2)$  and  $(p_2, q_2) = (3, 2)$ . If the interface is simple, the high order scheme is usually feasible. If a high order scheme is not feasible, the grid point is classified as an exceptional point. Instead, lower-order approximations should be applied at those exceptional points, see Fig. 3. The principles of adaptive-order strategy can now be stated as follows.

- When a grid point is not an interior point, we check the feasibility for the orders  $p_{1:2} = q_{1:2} = 2$  first. If it is not feasible, the grid point is an exceptional point and a lower-order approximation is applied.
- If it is feasible, the orders  $p_{1:2}, q_{1:2}$  will change in the dimension-by-dimension approach as well as in the inversion of the coupling equation or system. They are changed by the following criteria:
  1. The order of interpolation is increased by 1 in the region with a larger absolute value of  $a$ .
  2. If it is not feasible for the orders in the first criterion, the order of interpolation is increased by 1 in the region with a smaller absolute value of  $a$ .
  3. In the first and the second criteria, if there are two choices ( $x$ - or  $y$ -direction) in the inversion of the coupling system, the smaller one will be increased by 1. If they are the same, the choice is free (here we choose the  $x$ -direction in our code).
  4. If it is not feasible for the orders in the first and the second criteria, the order in the opposite region of the grid point is decreased by 1, i.e.,  $q_{1:2}$  is decreased by 1. If  $q_1$  or  $q_2$  is zero after the decreasing, the grid point is classified as an exceptional point and a lower-order approximation is applied.
  5. In the fourth criteria, if there are two choices ( $x$ - or  $y$ -direction) in the inversion of the coupling system, the larger one will be decreased by 1. If they are the same, the choice is free (here we choose the  $x$ -direction in our code).

Here the orders in the lower-order approximation are  $p_{1:2} = q_{1:2} = 1$ . The derivation of the lower-order approximation is similar to the CIM1 in [18]. The only difference is the adaptive-order strategy. Therefore, we only provide the relevant formulas for Fig. 3(a):

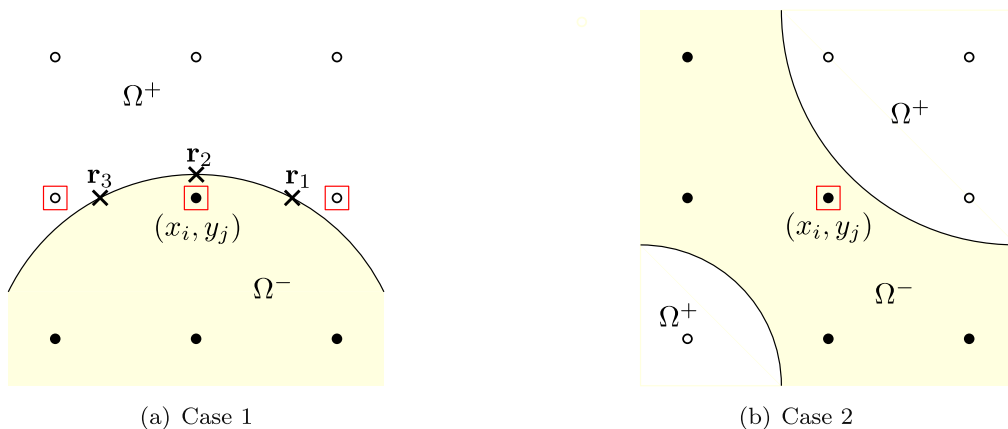


**Fig. 3.** Example of exceptional points. The regions colored by light yellow and white are  $\Omega^-$  and  $\Omega^+$ , respectively. The disks and circles are the grid points in  $\Omega^-$  and  $\Omega^+$ , respectively. The grid points marked by red squares are exceptional points. (For interpretation of the references to colour in this figure legend, the reader is referred to the web version of this article.)

- Dimension-by-dimension approach:

$$\frac{\partial u_{i+1/2,j}}{\partial x} \approx \frac{1}{h} \mathcal{D}_x^+ (u_{i-1+p_1^+,i+q_1^+,j}) + \sigma_1 \left[ a \frac{\partial u}{\partial x} \right]_{\mathbf{r}_1}; \tag{40}$$

$$\frac{\partial u_{i,j+1/2}}{\partial x} \approx \frac{1}{h} \mathcal{D}_y^+ (u_{i,j-1+p_2^+,j+q_2^+}) + \sigma_2 \left[ a \frac{\partial u}{\partial x} \right]_{\mathbf{r}_2}; \tag{41}$$

$$\frac{\partial u_{i-1/2,j}}{\partial x} \approx \frac{1}{h} \mathcal{D}_x^- (u_{i-1+p_1^-,i+q_1^-,j}) + \sigma_3 \left[ a \frac{\partial u}{\partial x} \right]_{\mathbf{r}_3}; \tag{42}$$

$$\frac{\partial u_{i,j-1/2}}{\partial y} \approx \frac{1}{h} (u_{i,j} - u_{i,j-1}). \tag{43}$$

Notice that  $p_{1,2}^\pm$  and  $q_{1,2}^\pm$  are adaptive-orders and all the first derivatives are in the domain  $\Omega^-$ .

- The decomposition of the jump data:

$$\left[ a \frac{\partial u}{\partial x} \right]_{\mathbf{r}_1} = ([a] \mathbf{t}_1 \cdot \mathbf{e}_1) \nabla u(\mathbf{r}_1^-) \cdot \mathbf{t}_1, \tag{44}$$

$$\left[ a \frac{\partial u}{\partial y} \right]_{\mathbf{r}_2} = ([a] \mathbf{t}_2 \cdot \mathbf{e}_2) \nabla u(\mathbf{r}_2^-) \cdot \mathbf{t}_2, \tag{45}$$

$$\left[ a \frac{\partial u}{\partial x} \right]_{\mathbf{r}_3} = ([a] \mathbf{t}_3 \cdot \mathbf{e}_1) \nabla u(\mathbf{r}_3^-) \cdot \mathbf{t}_3. \tag{46}$$

The unit tangential vectors  $\mathbf{t}_{1,3}$  are computed by the unit normal vectors  $\mathbf{n}_{1,3}$  at  $\mathbf{r}_{1,3}$ , respectively.

- The gradient terms:

$$\nabla u(\mathbf{r}_1^-) \approx \left[ \frac{\partial u_{i+1/2,j}}{\partial x}, \frac{\partial u_{i,j+1/2}}{\partial y} \right], \tag{47}$$

$$\nabla u(\mathbf{r}_2^-) \approx \left[ \frac{\partial u_{i+1/2,j}}{\partial x}, \frac{\partial u_{i,j+1/2}}{\partial y} \right], \tag{48}$$

$$\nabla u(\mathbf{r}_3^-) \approx \left[ \frac{\partial u_{i-1/2,j}}{\partial x}, \frac{\partial u_{i,j-1/2}}{\partial y} \right]. \tag{49}$$

- After substituting Eqs. (44)–(49) in Eqs. (40)–(43), we will get a  $4 \times 4$  linear system for  $(\partial/\partial x)u_{i\pm 1/2,j}$  and  $(\partial/\partial y)u_{i,j\pm 1/2}$ . If the determinant of the matrix is less than the tolerance, the adaptive-order strategy is applied. After inverting the matrix,  $(\partial/\partial x)u_{i\pm 1/2,j}$  and  $(\partial/\partial y)u_{i,j\pm 1/2}$  are expressed as the linear combination of the grid values. And the second order derivatives are approximated by:

$$\frac{\partial^2 u_{i,j}}{\partial x^2} \approx \frac{1}{h} \left( \frac{\partial u_{i+1/2,j}}{\partial x} - \frac{\partial u_{i-1/2,j}}{\partial x} \right), \tag{50}$$

$$\frac{\partial^2 u_{i,j}}{\partial y^2} \approx \frac{1}{h} \left( \frac{\partial u_{i,j+1/2}}{\partial y} - \frac{\partial u_{i,j-1/2}}{\partial y} \right). \tag{51}$$

The criteria of the adaptive-order strategy in the lower-order approximation is almost the same as those in the high order approximation expect the fourth and the fifth criteria. We cannot decrease the order in the lower-order approximation because the order is only one. If it is not feasible after increasing the orders in both regions, we refine the mesh size.

### 3. Eigenvalue problems in surface plasmon

Another application with sign-changed coefficients is plasmonics which also involves eigenvalue problems. It is considered to be the strongest interplay of both optical and electronic data transfer along a tiny metal [26]. It has found important applications in modern nano-technology such as magneto-optic data storage, microscopy, solar cells, sensors for detecting biological molecules, and plasmonic crystals [27]. Plasmonic crystals consist of periodic arrays of metallic and dielectric materials, and are useful to transmit sub-wavelength signals [28]. The physical properties of the wave guided mode in surface plasmon are discussed in reference [29]. However, convergence analysis is not provided. The derivation of the one-dimensional problem is clear if we integrate the order-altering strategy in the derivation. Therefore, we briefly state a sophisticated version of the two-dimensional eigenvalue problem here. For more details, we refer to [29].

Suppose the plasmonic crystal is homogeneous in the z-axis and the electromagnetic wave also propagates in this axial direction. The equations of the axial electric component  $E$  and magnetic component  $H$  are:

$$-\nabla_2 \cdot \left( \frac{\varepsilon \nabla_2 E}{\Lambda} \right) - \nabla_2 \times \left( \frac{k_z \nabla_2 H}{\omega \Lambda} \right) = \varepsilon E, \quad \text{in } \Omega \setminus \Gamma; \tag{52}$$

$$-\nabla_2 \cdot \left( \frac{\mu \nabla_2 H}{\Lambda} \right) + \nabla_2 \times \left( \frac{k_z \nabla_2 E}{\omega \Lambda} \right) = \mu H, \quad \text{in } \Omega \setminus \Gamma. \tag{53}$$

where  $\Lambda = \omega^2 \varepsilon \mu - k_z^2$ ;  $k_z$  is the axial wave number;  $\omega$  is the frequency; and  $\varepsilon$  and  $\mu$  are the permittivity and permeability of the medium, respectively. We assume that  $\Omega$  is a square. The Bloch boundary condition is applied at the cell boundary

$$E(x + L, y) = \exp(ik_x L)E(x, y), \tag{54}$$

$$E(x, y + L) = \exp(ik_y L)E(x, y), \tag{55}$$

$$H(x + L, y) = \exp(ik_x L)H(x, y), \tag{56}$$

$$H(x, y + L) = \exp(ik_y L)H(x, y), \tag{57}$$

where  $(k_x, k_y)$  is the Bloch wave vector, and  $L$  is the one side length of a cell. At the interface, the jump conditions for  $E$  and  $H$  are

$$[E]_\Gamma = 0, \tag{58}$$

$$[H]_\Gamma = 0, \tag{59}$$

$$\left[ \frac{\varepsilon}{\Lambda} \nabla_2 E \cdot \mathbf{n} \right]_\Gamma + \left[ \frac{k}{\omega \Lambda} \nabla_2 H \cdot \mathbf{t} \right]_\Gamma = 0, \tag{60}$$

$$\left[ \frac{\mu}{\Lambda} \nabla_2 H \cdot \mathbf{n} \right]_\Gamma - \left[ \frac{k}{\omega \Lambda} \nabla_2 E \cdot \mathbf{t} \right]_\Gamma = 0. \tag{61}$$

Here we adopt the Drude model for the permittivity of metals without the electron collision rate:

$$\varepsilon(x, y; \omega) = \varepsilon_0 \left( 1 - \frac{\omega_p^2}{\omega^2} \right), \quad \text{for } (x, y) \in \text{metal},$$

where  $\varepsilon_0$  is the permittivity constants in vacuum and  $\omega_p$  is the plasmon frequency. When the frequency  $\omega$  is under the plasmon frequency  $\omega_p$ , the permittivity changes its sign in the metal part. As a result, these plasmonic modes are highly localized and oscillate on the metal-dielectric interfaces.

Eqs. (52) and (53) can be formulated as an eigenvalue problem of the axial wavenumber  $k_z$ :

$$\left( \nabla_2^2 + \omega^2 \varepsilon \mu \right) E = k_z^2 E, \tag{62}$$

$$\left( \nabla_2^2 + \omega^2 \varepsilon \mu \right) H = k_z^2 H. \tag{63}$$

In this formulation, the structure of the metal-dielectric composite material is considered to be periodic, and the permittivity and permeability of the metallic component are functions of frequency. But another difficulty is that the jump conditions (60) and (61) involve the axial wave number. By introducing two auxiliary variables on the interface

$$J_E := [\varepsilon \nabla_2 E \cdot \mathbf{n}]_\Gamma, \tag{64}$$

$$J_H := [\mu \nabla_2 H \cdot \mathbf{n}]_\Gamma, \tag{65}$$

the jump conditions (60) and (61) can be formulated as a quadratic eigenvalue problem of axial wave number  $k_z$ :

$$C \left( \left[ \frac{1}{\mu} \nabla_2 E \cdot \mathbf{n} \right]_\Gamma + \frac{k_z}{\omega} \left[ \frac{1}{\varepsilon \mu} \nabla_2 H \cdot \mathbf{t} \right]_\Gamma \right) = k_z^2 J_E, \tag{66}$$

$$C \left( \left[ \frac{1}{\varepsilon} \nabla_2 H \cdot \mathbf{n} \right]_\Gamma - \frac{k_z}{\omega} \left[ \frac{1}{\varepsilon \mu} \nabla_2 E \cdot \mathbf{t} \right]_\Gamma \right) = k_z^2 J_H, \tag{67}$$

where  $C = \omega^2 \varepsilon^+ \varepsilon^- \mu^+ \mu^-$ . We drop the subindex of  $\nabla_2$  in the later derivation for simplicity.

We partition the unit cell  $\Omega = [0, L] \times [0, L]$  into  $N^2$  squares uniformly with mesh size  $h = \frac{L}{N}$ . The Cartesian grid points are  $(x_i, y_j) := (ih, jh)$ ,  $1 \leq i, j \leq N$ . We use the abbreviations  $E_{ij}$  for  $E(x_i, y_j)$  and  $E_{1:N, 1:N}$  for the unknowns  $(E_{1,1}, \dots, E_{N,N})$ . On the interface  $\Gamma$ , a set of uniformly distributed grids based on arc length on  $\Gamma$  is adopted. They are labeled by  $(\hat{x}_\ell, \hat{y}_\ell)$ ,  $\ell = 1, \dots, N_j$ . Notice that these coordinates are used only for the interfacial variables. The interface is represented by a levelset function. At these points, the auxiliary interfacial variables  $(J_{E,\ell}, J_{H,\ell})$  are defined. In an interior Cartesian grid point, Eqs. (62) and (63) are discretized by the standard central finite difference method. At a Cartesian grid point that is adjacent to the interface, the following coupling interface method is adopted. We only illustrate this idea for the case that  $\Gamma$  intersects both  $x$ - and  $y$ -directions. Suppose  $(x_i, y_j)$  is the grid point at which we want to derive a finite difference equation. Let  $\mathbf{r}_1 = (x_i + \alpha_1 h, y_j)$  and  $\mathbf{r}_2 = (x_i, y_j + \alpha_2 h)$  be the intersections of  $\Gamma$  and the  $x$  and  $y$ -axis from  $(x_i, y_j)$ ; and  $\hat{\mathbf{r}}_\ell = (\hat{x}_\ell, \hat{y}_\ell) = (x_i + \xi h, y_j + \eta h)$  be the closest interface grid point to  $(x_i, y_j)$ . Our goal is to derive the finite difference approximations for  $\nabla_2^2 E_{ij}$  and  $\nabla_2^2 H_{ij}$  in terms of the grid data and the interfacial variables. In this case, only the cross derivative terms can be approximated by the nearby points

$$\frac{\partial^2 E_{ij}}{\partial x \partial y} = \frac{E_{ij} - E_{ij-1} - E_{i-1,j} + E_{i-1,j-1}}{h^2} + O(h). \tag{68}$$

The difficulty is that the jump conditions are located at different locations. In order to derive a finite difference approximation for  $\frac{\partial^2 E_{ij}}{\partial x^2}$ , the jump data at a projected point on the grid line is considered:

$$\left[ \varepsilon \frac{\partial E}{\partial x} \right]_{(x_i+\xi h, y_j)} = \left[ \varepsilon \frac{\partial E}{\partial x} \right]_{\hat{\mathbf{r}}_\ell} - \eta h \left[ \varepsilon \frac{\partial^2 E}{\partial x \partial y} \right]_{\hat{\mathbf{r}}_\ell} + O(h^2). \tag{69}$$

We apply the one-dimensional method along the grid line  $y = y_j$  by considering two jump conditions (58) and (69):

$$\frac{\partial^2 E_{ij}}{\partial x^2} = \frac{1}{h^2} \mathcal{L}_x(E_{i-p_1+1:i+q_1, j}) + \frac{\sigma_1}{h} \left( \left[ \varepsilon \frac{\partial E}{\partial x} \right]_{\hat{\mathbf{r}}_\ell} - \eta h \left[ \varepsilon \frac{\partial^2 E}{\partial x \partial y} \right]_{\hat{\mathbf{r}}_\ell} \right) + O(h). \tag{70}$$

It is noted that the linear combination  $\mathcal{L}_x$  is dependent on  $\xi$ . Similarly, in the  $y$ -direction,

$$\frac{\partial^2 E_{ij}}{\partial y^2} = \frac{1}{h^2} \mathcal{L}_y(E_{i, j-p_2+1:j+q_2}) + \frac{\sigma_2}{h} \left( \left[ \varepsilon \frac{\partial E}{\partial y} \right]_{\hat{\mathbf{r}}_\ell} - \xi h \left[ \varepsilon \frac{\partial^2 E}{\partial x \partial y} \right]_{\hat{\mathbf{r}}_\ell} \right) + O(h). \tag{71}$$

The cross derivative term at  $\hat{\mathbf{r}}_\ell$  is approximated by

$$\frac{\partial^2 E}{\partial x \partial y}(\hat{\mathbf{r}}_\ell^-) = \frac{\partial^2 E_{ij}}{\partial x \partial y} + O(h), \quad \frac{\partial^2 E}{\partial x \partial y}(\hat{\mathbf{r}}_\ell^+) = \frac{\partial^2 E_{i+1, j+1}}{\partial x \partial y} + O(h), \tag{72}$$

where  $\frac{\partial^2 E_{i+1, j+1}}{\partial x \partial y}$  can be approximated by the linear combination of the nearby grid values, e.g.  $\frac{1}{h^2}(E_{i+2, j+2} - E_{i+2, j+1} - E_{i+1, j+2} + E_{i+1, j+1})$ , since  $(x_{i+1}, y_{j+1})$  is not near the interface. In the next step, the interfacial variables at interface grid points are used.

Re-expressing  $[\varepsilon \frac{\partial E}{\partial x}]_{\hat{\mathbf{r}}_\ell}$  and  $[\varepsilon \frac{\partial E}{\partial y}]_{\hat{\mathbf{r}}_\ell}$  in terms of normal and tangential derivatives of  $E$  at  $\hat{\mathbf{r}}_\ell$ :

$$\left[ \varepsilon \frac{\partial E}{\partial x} \right]_{\hat{\mathbf{r}}_\ell} = J_{E, \ell} \hat{\mathbf{n}} \cdot \mathbf{e}_1 + [\varepsilon] \hat{\mathbf{t}} \cdot \mathbf{e}_1 \nabla E(\hat{\mathbf{r}}_\ell^-) \cdot \hat{\mathbf{t}}, \tag{73}$$

$$\left[ \varepsilon \frac{\partial E}{\partial y} \right]_{\hat{\mathbf{r}}_\ell} = J_{E, \ell} \hat{\mathbf{n}} \cdot \mathbf{e}_2 + [\varepsilon] \hat{\mathbf{t}} \cdot \mathbf{e}_2 \nabla E(\hat{\mathbf{r}}_\ell^-) \cdot \hat{\mathbf{t}}, \tag{74}$$

where  $\hat{\mathbf{n}}$  and  $\hat{\mathbf{t}}$  are the unit normal and tangential vectors of  $\Gamma$  at  $\hat{\mathbf{r}}_\ell$ , respectively. Here we have used  $[\nabla E \cdot \hat{\mathbf{t}}]_{\hat{\mathbf{r}}_\ell} = 0$ . The one-side gradient can be expressed as

$$\nabla E(\hat{\mathbf{r}}_\ell^-) = \left[ \frac{1}{h}(E_{ij} - E_{i-1, j}) + \left(\frac{1}{2} + \xi\right)h \frac{\partial^2 E_{ij}}{\partial x^2} + \eta h \frac{\partial^2 E_{ij}}{\partial x \partial y} \right] + O(h^2). \tag{75}$$

By combining Eqs. (68)–(75), we deduce a coupling equation for the second order partial derivatives  $\frac{\partial^2 E_{ij}}{\partial x^2}$  and  $\frac{\partial^2 E_{ij}}{\partial y^2}$ .

$$\mathbf{M} \begin{bmatrix} \frac{\partial^2 E_{ij}}{\partial x^2} \\ \frac{\partial^2 E_{ij}}{\partial y^2} \end{bmatrix} = \frac{1}{h^2} \begin{bmatrix} \mathcal{L}_x(E_{i-p_1+1:i+q_1, j}) + \mathcal{T}_x(E_{i-1:i, j-1, j}, E_{i+1:i+2, j+1, j+2}) \\ \mathcal{L}_y(E_{i, j-p_2+1:j+q_2}) + \mathcal{T}_y(E_{i-1:i, j-1, j}, E_{i+1:i+2, j+1, j+2}) \end{bmatrix}, \tag{76}$$

where the matrix  $\mathbf{M}$  is

$$\mathbf{M} = \begin{bmatrix} 1 - \left(\frac{1}{2} + \xi\right)\sigma_1[\varepsilon](\hat{\mathbf{t}} \cdot \mathbf{e}_1)^2 & -\frac{1}{2}\sigma_1[\varepsilon](\hat{\mathbf{t}} \cdot \mathbf{e}_1)(\hat{\mathbf{t}} \cdot \mathbf{e}_2) \\ -\frac{1}{2}\sigma_2[\varepsilon](\hat{\mathbf{t}} \cdot \mathbf{e}_1)(\hat{\mathbf{t}} \cdot \mathbf{e}_2) & 1 - \left(\frac{1}{2} + \eta\right)\sigma_2[\varepsilon](\hat{\mathbf{t}} \cdot \mathbf{e}_2)^2 \end{bmatrix}. \tag{77}$$

If the determinant of  $\mathbf{M}$  is smaller than the tolerance, the adaptive-order strategy is applied. The criteria are the same as those in the previous section. Finally, we arrive at

$$\frac{\partial^2 E_{ij}}{\partial x^2} = \mathcal{L}_{E, x}(E_{i-1:i+2, j-1, j+2}, J_{E, \ell}) + O(h), \tag{78}$$

$$\frac{\partial^2 E_{ij}}{\partial y^2} = \mathcal{L}_{E, y}(E_{i-1:i+2, j-1, j+2}, J_{E, \ell}) + O(h), \tag{79}$$

where the symbols  $\mathcal{L}_{E, x}$  and  $\mathcal{L}_{E, y}$  represent the linear combinations. Then the finite difference scheme for  $\nabla^2 E_{ij}$  is

$$\nabla^2 E_{ij} = (\mathcal{L}_{E, x} + \mathcal{L}_{E, y})(E_{i-1:i+2, j-1, j+2}, J_{E, \ell}) + O(h). \tag{80}$$

Similarly, we can get the finite difference approximation for the  $H$  field:

$$\nabla^2 H_{ij} = (\mathcal{L}_{H, x} + \mathcal{L}_{H, y})(H_{i-1:i+2, j-1, j+2}, J_{H, \ell}) + O(h). \tag{81}$$

Discretize the interface conditions at interfacial grid points First, we express the left hand side of the interface conditions (66) and (67) in terms of the interfacial variables and one-side derivatives:

$$\begin{aligned} \left[ \frac{1}{\mu} \nabla E \cdot \hat{\mathbf{n}} \right]_{\hat{\mathbf{r}}_\ell} &= \frac{1}{\varepsilon_+ \mu_+} J_{E,\ell} + \frac{\varepsilon_- \mu_- - \varepsilon_+ \mu_+}{\varepsilon_+ \mu_+ \mu_-} \nabla E(\hat{\mathbf{r}}_\ell^-) \cdot \hat{\mathbf{n}}, \\ \left[ \frac{1}{\varepsilon \mu} \nabla H \cdot \hat{\mathbf{t}} \right]_{\hat{\mathbf{r}}_\ell} &= \frac{\varepsilon_- \mu_- - \varepsilon_+ \mu_+}{\varepsilon_+ \varepsilon_- \mu_+ \mu_-} \nabla H(\hat{\mathbf{r}}_\ell^-) \cdot \hat{\mathbf{t}}, \\ \left[ \frac{1}{\varepsilon} \nabla H \cdot \hat{\mathbf{n}} \right]_{\hat{\mathbf{r}}_\ell} &= \frac{1}{\varepsilon_+ \mu_+} J_{H,\ell} + \frac{\varepsilon_- \mu_- - \varepsilon_+ \mu_+}{\mu_+ \varepsilon_+ \varepsilon_-} \nabla H(\hat{\mathbf{r}}_\ell^-) \cdot \hat{\mathbf{n}}, \\ \left[ \frac{1}{\varepsilon \mu} \nabla E \cdot \hat{\mathbf{t}} \right]_{\hat{\mathbf{r}}_\ell} &= \frac{\varepsilon_- \mu_- - \varepsilon_+ \mu_+}{\varepsilon_+ \varepsilon_- \mu_+ \mu_-} \nabla E(\hat{\mathbf{r}}_\ell^-) \cdot \hat{\mathbf{t}}. \end{aligned}$$

These normal and tangential derivatives can be approximated by the derivatives along the  $x$  and  $y$ -direction. For instance,  $\nabla E(\hat{\mathbf{r}}_\ell^-)$  can be approximated in terms of nearby grid data and the interfacial data by using (68), (75), (78) and (79). Finally, the interfacial operators in (66) and (67) are approximated by linear combinations of grid data and interfacial variables:

$$C \left[ \frac{1}{\mu} \nabla E \cdot \hat{\mathbf{n}} \right]_{\hat{\mathbf{r}}_\ell} = \mathcal{J}_{E,\hat{\mathbf{n}}} (E_{i-1:i+2j-1j+2}, J_{E,\ell}) + O(h^2), \tag{82}$$

$$\frac{C}{\omega} \left[ \frac{1}{\varepsilon \mu} \nabla H \cdot \hat{\mathbf{t}} \right]_{\hat{\mathbf{r}}_\ell} = \mathcal{J}_{H,\hat{\mathbf{t}}} (H_{i-1:i+2j-1j+2}, J_{H,\ell}) + O(h^2), \tag{83}$$

$$C \left[ \frac{1}{\varepsilon} \nabla H \cdot \hat{\mathbf{n}} \right]_{\hat{\mathbf{r}}_\ell} = \mathcal{J}_{H,\hat{\mathbf{n}}} (H_{i-1:i+2j-1j+2}, J_{H,\ell}) + O(h^2), \tag{84}$$

$$\frac{C}{\omega} \left[ \frac{1}{\varepsilon \mu} \nabla E \cdot \hat{\mathbf{t}} \right]_{\hat{\mathbf{r}}_\ell} = \mathcal{J}_{E,\hat{\mathbf{t}}} (E_{i-1:i+2j-1j+2}, J_{E,\ell}) + O(h^2), \tag{85}$$

where the symbols  $\mathcal{J}_{E,\hat{\mathbf{n}}}$ ,  $\mathcal{J}_{H,\hat{\mathbf{t}}}$ ,  $\mathcal{J}_{H,\hat{\mathbf{n}}}$  and  $\mathcal{J}_{E,\hat{\mathbf{t}}}$  represent the linear combinations. The discretized interface conditions become

$$\mathcal{J}_{E,\hat{\mathbf{n}}} (E_{i-1:i+2j-1j+2}, J_{E,\ell}) + k \mathcal{J}_{H,\hat{\mathbf{t}}} (H_{i-1:i+2j-1j+2}, J_{H,\ell}) = k^2 J_{E,\ell} + O(h^2), \tag{86}$$

$$\mathcal{J}_{H,\hat{\mathbf{n}}} (H_{i-1:i+2j-1j+2}, J_{H,\ell}) - k \mathcal{J}_{E,\hat{\mathbf{t}}} (E_{i-1:i+2j-1j+2}, J_{E,\ell}) = k^2 J_{H,\ell} + O(h^2). \tag{87}$$

Combining the discretization (80), (81), (86) and (87) with the Bloch boundary condition, we arrive a quadratic eigenvalue problem:

$$\mathbf{A}_{\text{mix}} \mathbf{U}_{\text{mix}} + k \mathbf{B}_{\text{mix}} \mathbf{U}_{\text{mix}} = k^2 \mathbf{U}_{\text{mix}},$$

where  $\mathbf{A}_{\text{mix}}$  and  $\mathbf{B}_{\text{mix}}$  are  $2(N^2 + N_j) \times 2(N^2 + N_j)$  matrices and

$$\mathbf{U}_{\text{mix}} = [E_{1:N,1:N}, H_{1:N,1:N}, J_{E,1:N_j}, J_{H,1:N_j}]^T.$$

We solve this quadratic eigenvalue problem by doubling the matrix to transfer the problem to a standard eigenvalue problem:

$$\begin{bmatrix} \mathbf{0} & \mathbf{I} \\ \mathbf{A} & \mathbf{B} \end{bmatrix} \begin{bmatrix} \mathbf{U}_{\text{mix}} \\ k \mathbf{U}_{\text{mix}} \end{bmatrix} = k \begin{bmatrix} \mathbf{U}_{\text{mix}} \\ k \mathbf{U}_{\text{mix}} \end{bmatrix}.$$

### 4. Numerical results

Below, we perform convergence tests for one- and two-dimensional problems.

#### 4.1. Convergence validation for population dynamics

For the one-dimensional problem, Eq. (6) with piecewise constant, the exact solution can be easily derived:

$$u(x) = \begin{cases} c_1 e^{\zeta_1 x} + c_2 e^{-\zeta_1 x}, & x < \hat{x}, \\ c_3 e^{\zeta_2 x} + c_4 e^{-\zeta_2 x}, & x > \hat{x}, \end{cases} \tag{88}$$

where  $\zeta_1 = \sqrt{\lambda m^- / a^-}$  and  $\zeta_2 = \sqrt{\lambda m^+ / a^+}$ . The Robin boundary conditions (Eqs. (7) and (8)) and interface conditions (Eqs. (9) and (10)) give four linear equations for the undetermined coefficients  $c_{1:4}$ . The determinant of the four equations is a function of  $\lambda, \hat{x}, L, \gamma, m^\pm$  and  $a^\pm$ . When  $\hat{x}, L, \gamma, m^\pm, a^\pm$  are given, a numerical method is used to find  $\lambda$ , which makes the determinant zero in order to get a nontrivial solution of  $c_{1:4}$ . The eigenfunction  $c_{1:4}$  is normalized by unity  $L^2$  norm of  $u$ . In the numerical tests, we only show the result with Dirichlet boundary condition. The results with other boundary conditions are similar.

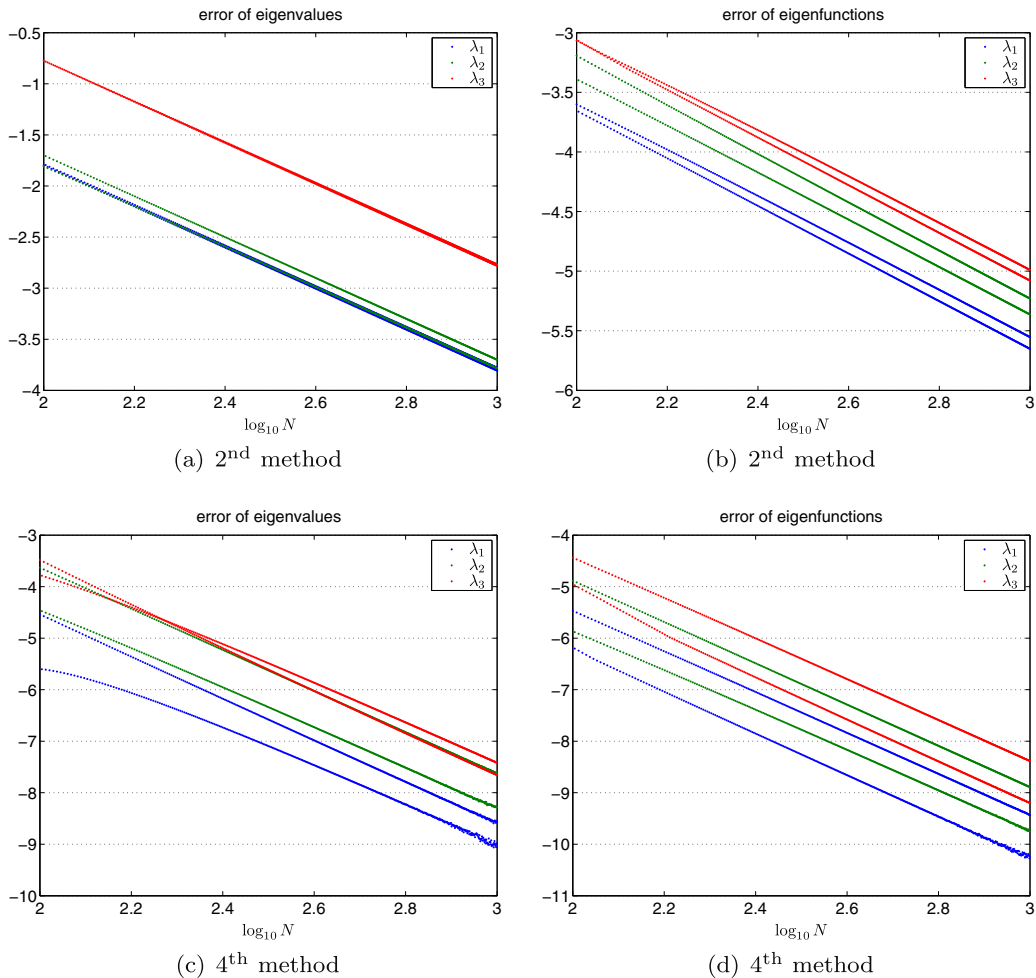


**Fig. 4.** Log–log plots of the error in Example 1 versus the number of mesh  $N$ . In this case,  $\Omega = [0, 1]$ ,  $\hat{x} = 0.5$ . Dirichlet boundary condition is applied. The coefficients is chosen to be  $a^- = -1$ ,  $a^+ = 1$  and the growth rates are  $m^- = 2$ ,  $m^+ = 1$ .  $N$  varies from 100 to 1000 with  $\Delta N = 1$ . (a) and (b) are computed by second order method while (c) and (d) are computed by fourth order method. The blue, green and red dots represent the errors of the first, second and third eigenvalues and eigenfunctions, respectively. (For interpretation of the references to colour in this figure legend, the reader is referred to the web version of this article.)

**Example 1.** For the first example, the interface is set to the center of  $\Omega = [0, 1]$ . We choose  $a^- = -1$ ,  $a^+ = 1$ ,  $m^- = 2$  and  $m^+ = 1$ . When the number of mesh  $N$  is odd, the linear combinations of discretization at  $(N - 1)/2$  and  $(N + 1)/2$  cannot be solved with the same order approximation on each side of the interface, i.e.  $p = q$ . The adaptive-order strategy is applied when  $N$  is odd. Therefore, the effect of adaptive-order strategy can be shown. The exact eigenvalues with 10-digits are  $\lambda_1 = -33.52204426$ ,  $\lambda_2 = 56.46168338$  and  $\lambda_3 = 104.7908422$ . They are found by using the “fzero” subroutine in MATLAB to test if the determinant is zero. The log–log plot of errors of eigenvalues and eigenfunctions versus  $N$  is shown in Fig. 4. The error of eigenfunction is measured with  $L^\infty$  norm of the difference between the exact and computed eigenfunctions. For each eigenvalue, the errors are split to two lines. They correspond to even and odd numbers of mesh. The errors produced by different order approximation are almost the same order. This shows that the adaptive-order strategy maintains the accuracy and solves the nonexistence problem of linear combination. Regarding accuracy, the second order method is computed by setting  $p, q \geq 2$ , and the fourth method is computed by setting  $p, q \geq 4$ . In all sub-figures in Fig. 4, the width of the  $x$ -axis is 1, so the slope in the lines is the difference in the  $y$ -axis. We can see that the slopes of the lines in Fig. 4(a), (b) are almost  $-2$ , and the slopes of lines in Fig. 4(c), (d) are almost  $-4$ . The second and fourth order convergences of the eigenvalues and eigenfunction are clearly shown.

**Example 2.** In the second example, the location of the interface is chosen to be an irrational number  $\hat{x} = 5 \ln 5/16$  near the center of  $\Omega$ . It will be located at different reference places in a cell when  $N$  varies. More precisely, if  $\hat{x} = x_i + \alpha h$  for some integer  $i$ ,  $0 \leq \alpha < 1$ , the reference location  $\alpha$  varies with  $N$ . The situation is closer to a two-dimensional case with a complex interface. The other parameters are the same as the first example. The log–log plot of errors of eigenvalues and eigenfunctions

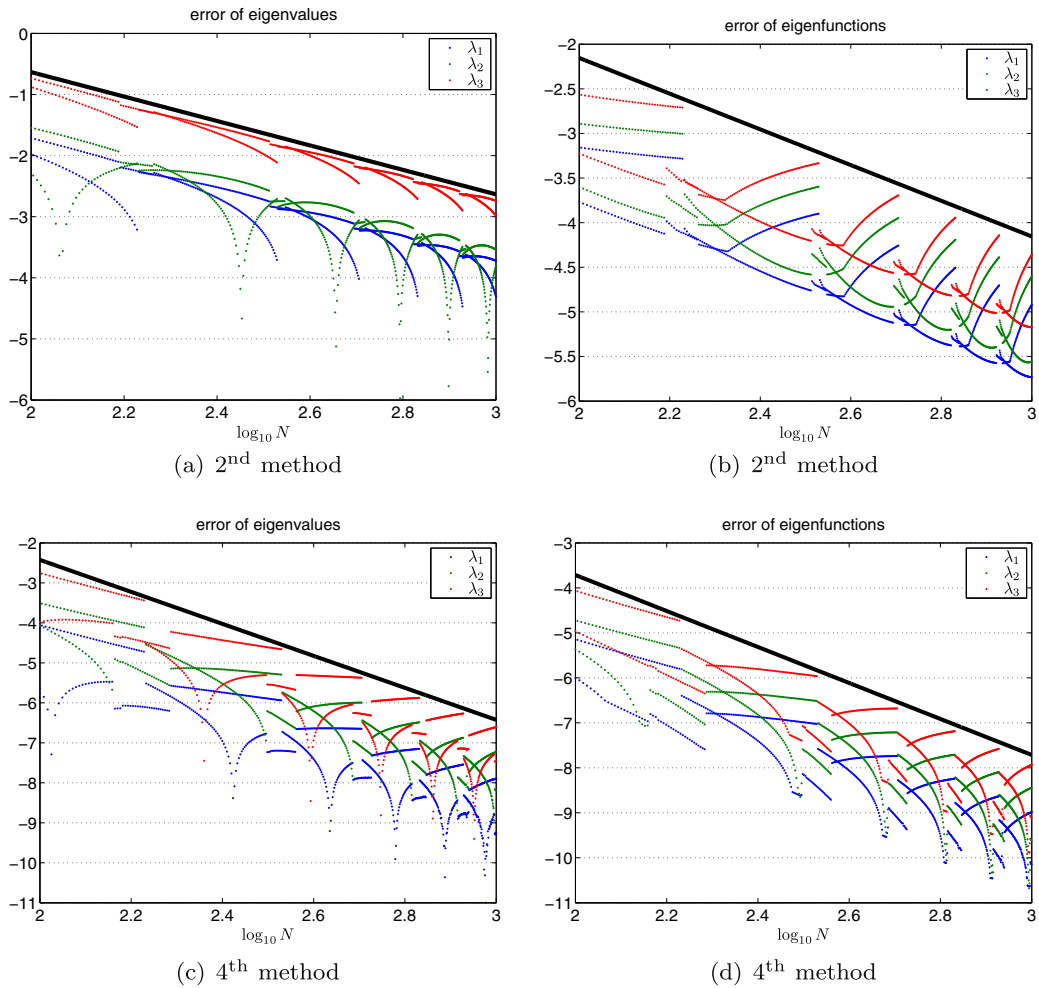


**Fig. 5.** Log–log plots of the error in Example 2 versus the number of mesh  $N$ . In this case,  $\Omega = [0,1]$ ,  $\hat{x} = 5 \ln 5/16$ . The Dirichlet boundary condition is applied. The coefficients are chosen to be  $a^- = -1$ ,  $a^+ = 1$  and the growth rates are  $m^- = 2$ ,  $m^+ = 1$ .  $N$  varies from 100 to 1000 with  $\Delta N = 1$ . (a) and (b) are computed by the second order method, while (c) and (d) are computed by the fourth order method. The blue, green and red dots represent the errors of the first, second, and third eigenvalues and eigenfunctions, respectively. The black lines are reference lines. The slopes of reference lines are  $-2$  in (a), (b) and  $-4$  in (c), (d). (For interpretation of the references to colour in this figure legend, the reader is referred to the web version of this article.)

versus  $N$  are shown in Fig. 5. An interesting thing is that the curves follow a specific pattern. The pattern is almost the same as the error of using a rational number to approximate an irrational number, since the error depends on the reference location  $\alpha$ . Even though the curves are not a straight line, the convergence order somehow can be read from the reference lines. The slopes of the reference lines are  $-2$  in Fig. 5(a), (b) and  $-4$  in Fig. 5(c), (d). The second and fourth order convergences of this example are clearly shown.

Another issue is the condition number of the matrix. We use the scaled condition number, which is the condition number divided by  $N^2$ , since the condition number of the matrix will grow with the factor  $N^2$ . Fig. 6 shows the log–log plots of the scaled condition number versus the number of mesh  $N$ . The blue dots and the red circles are the scaled condition numbers without and with the adaptive-order strategy, respectively. Here the adaptive-order strategy is applied when the tolerance is 0.15. When the adaptive-order strategy is applied, the scaled condition number is under controlled and about 0.01 to 0.1 times the original. It shows that the condition number of the discretization matrix is controlled by the adaptive-order strategy. In addition, the errors of eigenvalues and eigenfunctions are also smaller when the adaptive-order strategy is applied.

**Example 3.** The third example is a two-dimensional problem. The domain is set to be  $\Omega = [-\pi, \pi] \times [-\pi, \pi]$ . The interface is a circle,  $x^2 + y^2 - \pi^2/4 = 0$ , in the center of  $\Omega$ . Inside the circle is  $\Omega^-$  and outside is  $\Omega^+$ . The coefficients and growth rate are set to be  $a^- = 1$ ,  $a^+ = -10$  and  $m^- = m^+ = 1$ . The number of intervals in each side ( $N$ ) varies from 40 to 200 with  $\Delta N = 10$ . When constructing the polynomials on both sides of interface, the orders of polynomials are chosen to be not less than two. But for a two-dimensional eigenvalue problem, the nontrivial exact solution is hard to find. Therefore, a solution with a very fine

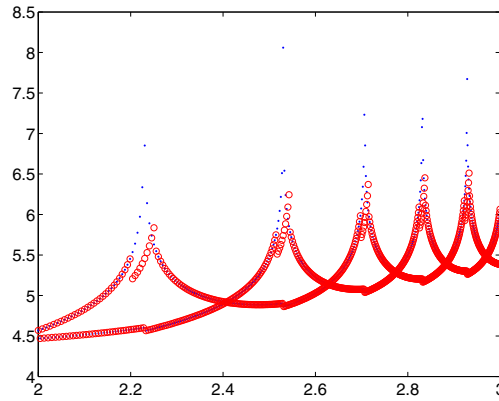


**Fig. 6.** Log–log plots of the scaled condition number in Example 2 versus the number of mesh  $N$ . X-axis:  $\log_{10}N$ , Y-axis:  $\log_{10}(\text{condition number of the discretization matrix}/N^2)$ .  $N$  varies from 100 to 1000 with  $\Delta N = 1$ . The blue dots and the red circles are the scaled condition numbers without and with the adaptive-order strategy, respectively. Here the tolerance in the adaptive-order strategy is 0.15. (For interpretation of the references to colour in this figure legend, the reader is referred to the web version of this article.)

grid is used as the exact solution instead. The convergence order is computed by comparison with the solution with a very fine grid. But this will cause error in the convergence order, which is estimated by the following. Suppose that the exact solution exists and the exact eigenvalue is  $\lambda_*$ . The eigenvalue computed by a numerical method with mesh size  $h$  is labeled by  $\lambda_h$ . A convergence order  $m_*$  is defined by

$$|\lambda_h - \lambda_*| \leq Ch^{m_*}. \tag{89}$$

Let  $h_0$  be the mesh size of the very fine grid. Then we have

$$|\lambda_h - \lambda_{h_0}| \leq C(h^{m_*} + h_0^{m_*}). \tag{90}$$

The computed convergence order  $m_0$  corresponding to  $h_0$  is determined by a least square method

$$m_0 = \text{LS}(\{\log h_i\}_{i=1}^{N_h}, \{\log |\lambda_{h_i} - \lambda_{h_0}|\}_{i=1}^{N_h}), \tag{91}$$

where

$$\text{LS}(\{v_i\}_{i=1}^{N_h}, \{\delta_i\}_{i=1}^{N_h}) = \frac{\sum_{i=1}^{N_h} (v_i - \bar{v})(\delta_i - \bar{\delta})}{\sum_{i=1}^{N_h} (v_i - \bar{v})^2}. \tag{92}$$

Here the notation  $\bar{v}$  is the average of  $v$ . Suppose  $m_*$  can be approximated by a least square method of

$$m_* = \text{LS}(\{\log h_i\}_{i=1}^{N_h}, \{\log |\lambda_{h_i} - \lambda_*|\}_{i=1}^{N_h}). \tag{93}$$

Then the relation of  $m_*$  and  $m_0$  is

$$|m_* - m_0| \leq \frac{\sum_{i=1}^{N_h} |v_i - \bar{v}| \left(\frac{h_0}{h_i}\right)^{m_*}}{\sum_{i=1}^{N_h} |v_i - \bar{v}|^2}, \tag{94}$$

where  $v_i = \log h_i$ . The real convergence order  $m_*$  is a range that satisfies Eq. (94).

By searching  $m_*$  in Eq. (94), the maximum and the minimum of the convergence order for this two-dimensional example is listed in Table 3. It shows that if the exact eigenvalues exist and the order can be found by comparison with the exact eigenvalues, the eigenvalue computed by our method is second order convergence. In addition, the eigenfunction and the convergence result are shown in Fig. 7.

**Example 4.** This example is a test for complex interfaces. All the parameters are the same as in Example 3 except the interface, which is described in the polar coordinate

$$\phi(r, \theta) = r - \pi \left( 1 + 0.15 \sin \left( 5 \left( \theta - \frac{\pi}{4} \right) \right) \right) / 2 = 0,$$

where  $r = \sqrt{x^2 + y^2}$ ,  $\theta = \tan^{-1}(y/x)$ . In order to capture the shape of the interface and test the robustness of the method,  $N$  varies from 80 to 200 with  $\Delta N = 1$ . Fig. 8 shows the first and second eigenfunctions and the convergence result. By Eq. (94), the proper convergence order of  $\lambda_1$  and  $\lambda_2$  is in [2.1861, 2.4091] and [2.0260, 2.2971], respectively. It shows that a second order convergence is achieved. Due to the complexity of the interface, exceptional points are found for some  $N$  in [80, 200] and the high order approximation is not feasible at those exceptional points. Here, we use lower-order

**Table 3**  
The convergence order estimated by Eq. (94) for Example 3.

	Minimum of $m^*$	Maximum of $m^*$
1st eigenvalues	1.9968	2.1306
2nd eigenvalues	1.9907	2.1256
3rd eigenvalues	2.0059	2.1382

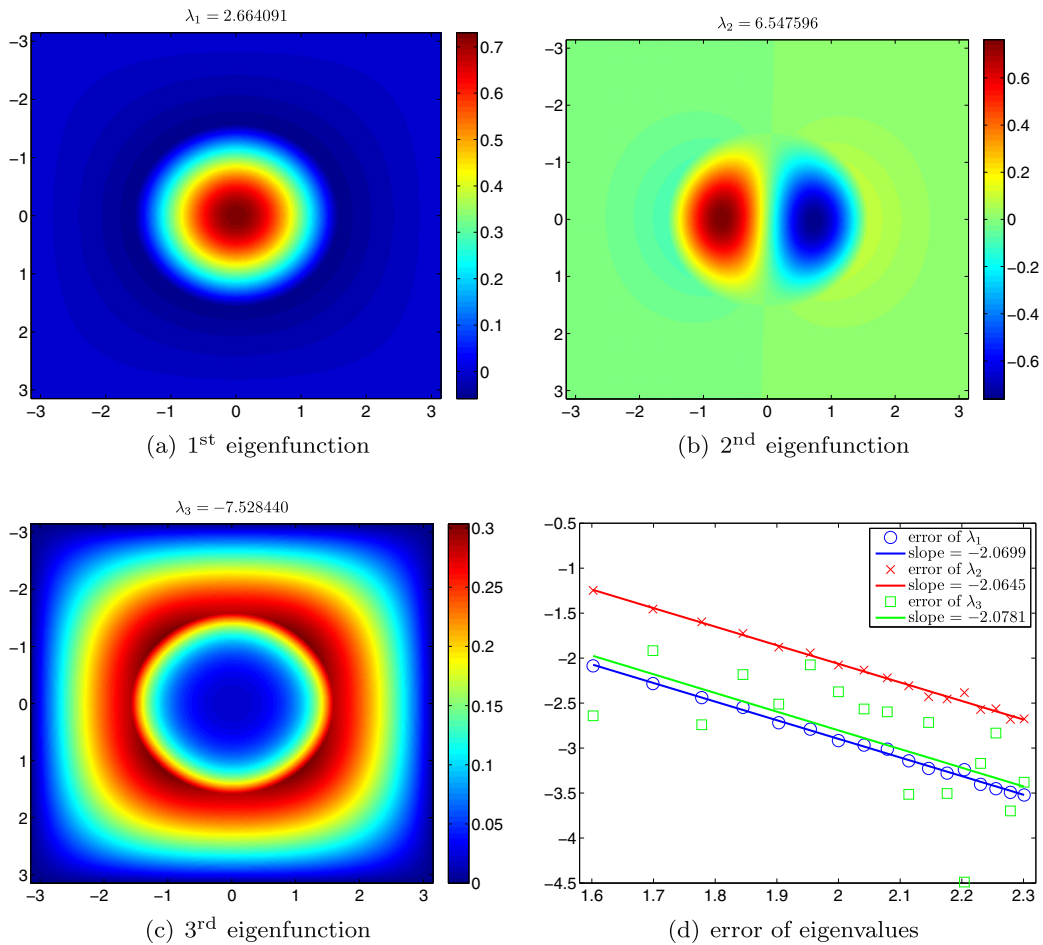


**Fig. 7.** Eigenfunctions (a,b,c) in Example 3 and the log–log plot (d) of the error of eigenvalues versus the number of mesh in one side. The eigenfunctions are computed with  $N = 640$ . The domain  $\Omega$  is set to be  $[-\pi, \pi] \times [-\pi, \pi]$ . The interface,  $\Gamma : (x^2 + y^2) - \pi^2/4 = 0$ , is a circle in the center of  $\Omega$ . Inside the circle is  $\Omega^-$  and outside is  $\Omega^+$ . The parameters are  $m^- = m^+ = 1$ ,  $a^- = 1$ ,  $a^+ = -10$ . The number of mesh in one side ( $N$ ) varies from 40 to 200 with  $\Delta N = 10$ . It is a second order method by setting  $p, q \geq 2$ .

approximations at the exceptional points. Since the number of exceptional points is  $O(1)$  at a fixed  $N$ , the convergence of eigenvalue is still of second order. However, when exceptional points occur, the errors are larger.

#### 4.2. Convergence validation for surface plasmon

In the numerical tests, we choose  $\epsilon^+ = \epsilon_0$ , the permittivity of air. The following non-dimensional transformation is used:

$$\tilde{\omega} = \frac{\omega L}{2\pi c}, \quad \tilde{\omega}_p = \frac{\omega_p L}{2\pi c}, \quad \tilde{k} = \frac{kL}{2\pi}, \quad \tilde{x} = \frac{2\pi x}{L}, \quad \tilde{y} = \frac{2\pi y}{L}.$$

where  $c = \sqrt{1/(\epsilon_0 \mu_0)}$  is the speed of light in vacuum;  $\mu_0$  is the permeability constants in vacuum. Since surface plasmon waves often happen on the nano scale, the magnitudes of  $\omega_p L$  and  $c$  are of the same order; we choose  $\tilde{\omega}_p = 1$ . For computation, we rescale  $E, H, J_E$  and  $J_H$  so that the rescaled quantities are of the same order of magnitude.

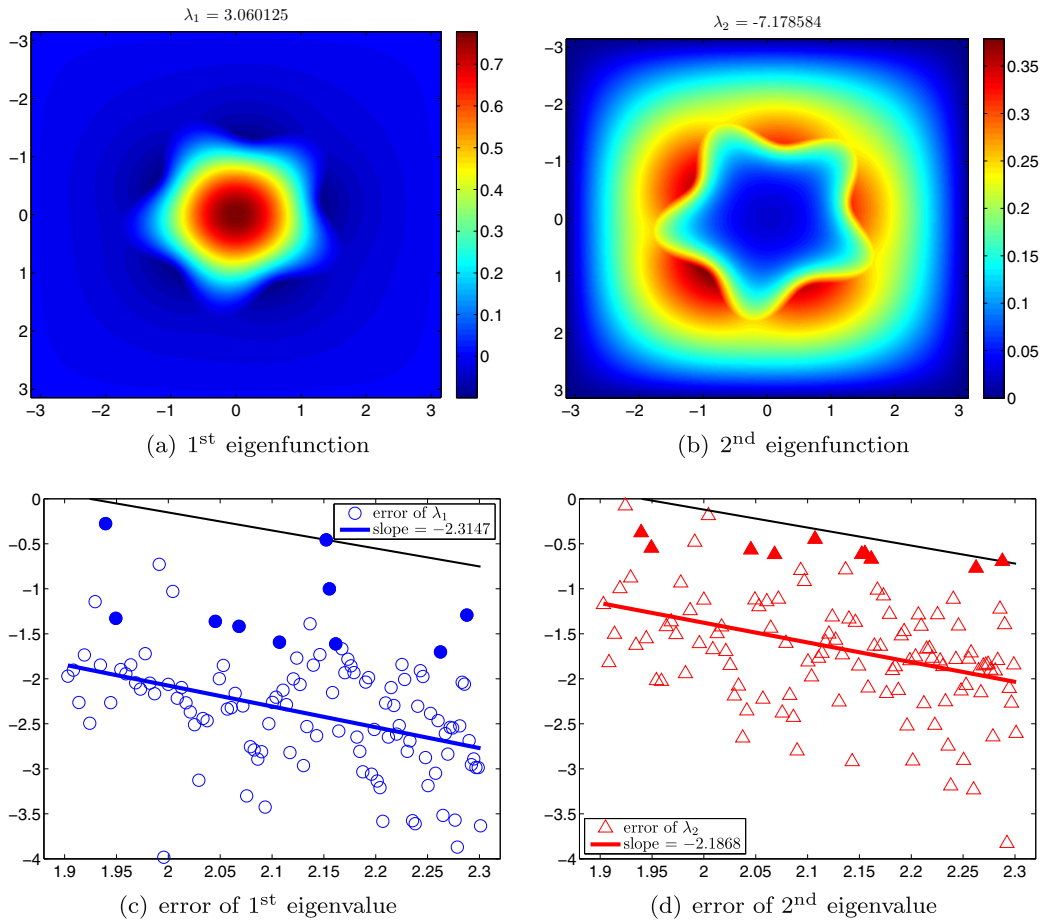


**Fig. 8.** Eigenfunctions (a,b) in Example 4 and their log–log plots (c,d) of the error of eigenvalues versus the number of mesh in one side. The eigenfunctions are computed with  $N = 640$ . The domain  $\Omega$  is set to be  $[-\pi, \pi] \times [-\pi, \pi]$ . The interface  $\Gamma$  is described by  $\phi(r, \theta) = r - \pi(1 + 0.15\sin(5(\theta - \pi/4)))/2 = 0$  in polar coordinate. Inside the flower-like interface is  $\Omega^-$  and outside is  $\Omega^+$ . The parameters are  $m^- = m^+ = 1$ ,  $a^- = 1$ ,  $a^+ = -10$ . The number of mesh in one side ( $N$ ) varies from 80 to 200 with  $\Delta N = 1$ . Hollow symbols in (c) and (d) are computed by using the high order approximation. The exceptional point does not occur at those  $N$ 's. Solid symbols in (c) and (d) are computed by using the lower-order approximation at the exceptional points. The slopes of the black lines in (c) and (d) are  $-2$ .

$$\tilde{E} = \sqrt{\epsilon_0}E, \quad \tilde{H} = \sqrt{\mu_0}H, \quad \tilde{J}_E = h[\epsilon \nabla \tilde{E} \cdot \mathbf{n}], \quad \tilde{J}_H = h[\mu \nabla \tilde{H} \cdot \mathbf{n}].$$

Notice that  $\tilde{J}_E$  and  $\tilde{J}_H$  are chosen to be mesh dependent, as the solution  $(E, H)$  decays exponentially on both sides of the interfaces. The best thickness we can compute is of order  $h$ . This leads to  $[\nabla E \cdot \mathbf{n}]$  and  $[\nabla H \cdot \mathbf{n}]$  being  $O(h^{-1})$ . This is why we scale  $\tilde{J}_E$  and  $\tilde{J}_H$  in this way.

**Example 5.** A benchmark problem is to compute the surface plasmonic wave in a layer structure, where an analytical solution is available [20]. We shall compute the case when  $\tilde{\omega} = 0.7$ , which is very close to the surface plasmonic frequency  $\tilde{\omega}_{sp} = 1/\sqrt{2}$ . In this case, there are two surface plasmonic wave modes: a symmetric one and an anti-symmetric one; see Fig. 9. The peaks occur at the interfaces and the surface plasmon modes are highly localized. Computation of such solutions can reflect the quality of a numerical method. These analytical solutions and the corresponding eigenvalues  $\tilde{k}$  are obtained from the analytical formula in [20] using Maple with 40 significant digits. Here, we choose the filled-in ratio of metal to be 40%. The corresponding eigenvalue  $\tilde{k}$  is

$$\tilde{k}_{\text{exact}} = \begin{cases} 3.5446728105477856717711645184356830360 & \text{symmetric case,} \\ 3.5245741559036641558099416554137229943 & \text{anti-symmetric case.} \end{cases}$$

To view the convergence behavior of  $\tilde{k}_{\text{num}}(N)$ , we calculate the true errors

$$e(N) := |\tilde{k}_{\text{num}}(N) - \tilde{k}_{\text{exact}}|,$$

for  $N$  ranging from 100 to 1000 with increment  $\Delta N = 1$ . Fig. 10 is the log–log plot of these errors versus  $N$ . Notice that the relative location of the interface  $\hat{x}$  in a cell varies in  $N$ . Let  $\alpha = (\hat{x} - x_i)/h$  be this relative position. We observe that the worst

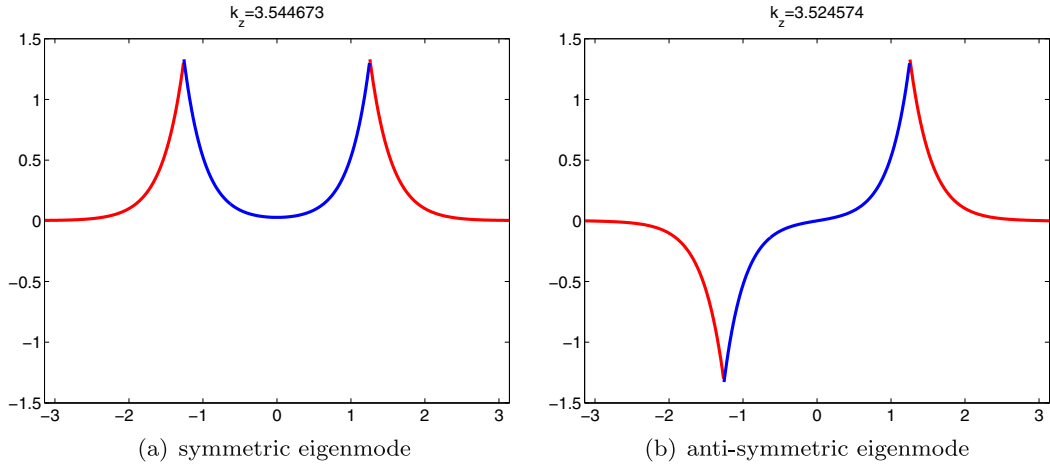


**Fig. 9.** The symmetric and anti-symmetric eigenmodes of the layer structure in Example 5 corresponding to the case when  $\bar{\omega} = 0.7$ . The filling ratio is 40%. This is computed from the analytic formula in [20]. These plasmonic modes are normalized with unity  $L^2$  norm in a unit cell.

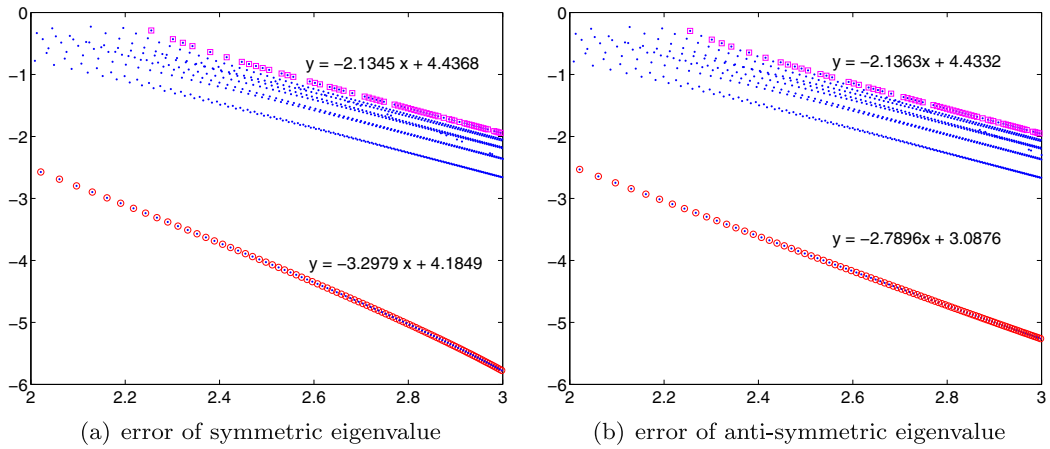


**Fig. 10.** The log–log plot of the error of the eigenvalue  $k_z$  in Example 5 corresponding to the case when  $\bar{\omega} = 0.7$  versus the number of grid points  $N$  for  $N$  ranging from 100 to 1000 with  $\Delta N = 1$ . The relative position of the interface  $\alpha$  varies in  $N$ . The red circle marks those cases with  $\alpha = 0.5$ , whereas the magenta square marks those cases with  $\alpha = 0$ . The least square fit of the red circles is  $y = -3.2979x + 4.1849$ , whereas the least square fit of the magenta squares is  $y = -2.1345x + 4.4368$ , a second order convergence. (For interpretation of the references to colour in this figure legend, the reader is referred to the web version of this article.)

cases happen when  $\alpha = 0$  (marked by magenta squares), where a second order accuracy is still achieved. When  $\alpha = 0.5$ , the error is much reduced and results in a third order accuracy. Evidently, this is due to the symmetry of the grids with respect to the interface, and certain cancellation occurs in the ACIM. Fig. 11 is the point-wise errors of these two eigenmodes computed by the ACIM with grid number  $N = 1000$ . These plasmonic modes are normalized with unity  $L^2$  norm in a unit cell. We see that the relative error in  $L^\infty$  is about  $10^{-5}$ .

We give two examples for convergence validation for two-dimensional surface plasmonic problems. One is the oblique layer structure, while the other is the circular dielectric hole. For the first one, we have an analytic solution for comparison. For the second one, no analytic solution is available. We use the fine grid result as a referenced solution for comparison. For both cases, the ACIM achieves second order convergence.

**Example 6 (Convergence validation for an oblique layer structure).** We rotate the previous one-dimensional layer structure to obtain a two dimensional analytical solution for comparison. In the previous one-dimensional layer structure, the eigenmode has the form:

$$\mathbf{E} = e^{i(k_x x + k_z z - \omega t)} (0, 0, E_z(x)),$$

$$\mathbf{H} = e^{i(k_x x + k_z z - \omega t)} (0, H_y(x), 0),$$

where  $k_x$  is the Bloch wave number,  $(0, 0, k_z)$  is the propagation wave vector, and  $\omega$  is the frequency. The  $E_z$  field of the two eigenmodes  $E_z(x)$  is shown in Fig. 9. The corresponding  $H_y$  field can be computed from  $E_z$  by the Maxwell equations.

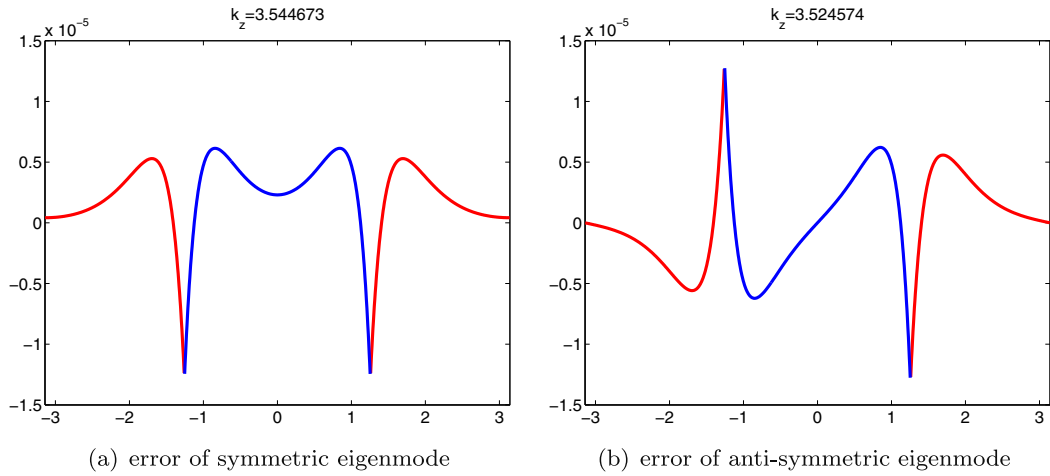


**Fig. 11.** The errors of the  $E$ -field (i.e.  $E_{\text{num}} - E_{\text{exact}}$ ) of these eigenmodes computed by the ACIM with grid number  $N = 1000$  corresponding to the case when  $\tilde{\omega} = 0.7$  in Example 5. The exact eigenmodes are shown in Fig. 9. These numerical plasmonic modes are also normalized with unity  $L^2$  norm in a unit cell. The relative point-wise error is about  $10^{-5}$ .

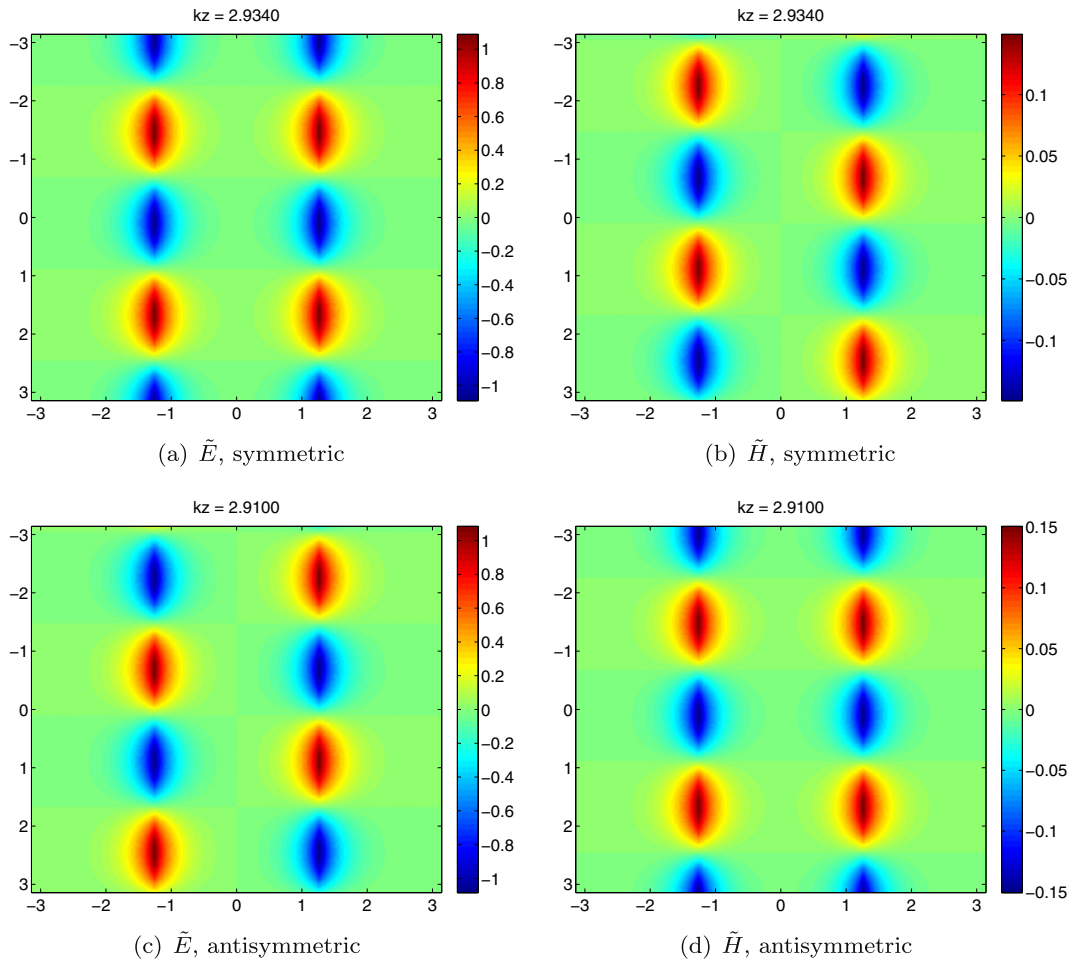


**Fig. 12.** The eigenmodes of the oblique layer structure computed by the two dimensional ACIM with  $N = 320$  in Example 6. The filling ratio is 40%,  $\tilde{\omega} = 0.7$ ,  $k_x = 0$ ,  $k_y = 2$ . These plasmonic wave modes are normalized with unity  $L^2$  norm in a unit cell.

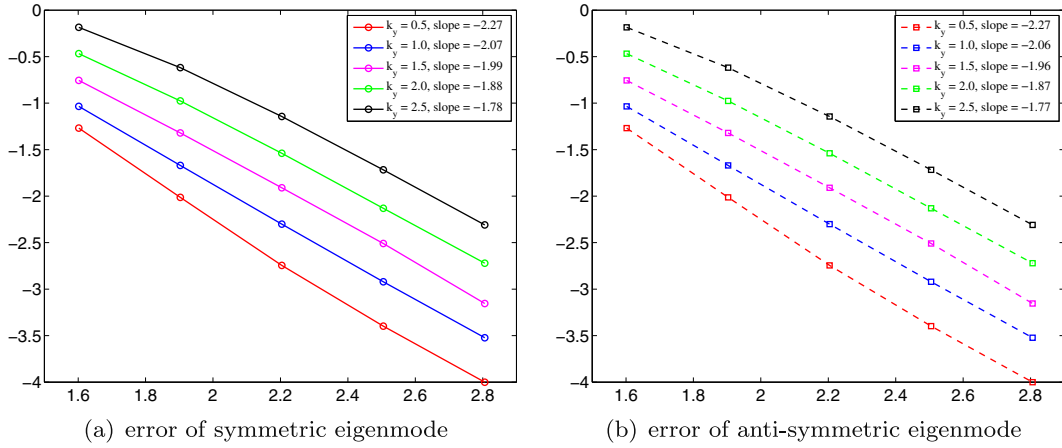


**Fig. 13.** The log-log plot of the error of the eigenvalue computed by two-dimensional ACIM versus the number of grid points  $N$  for  $N$  ranging from 40 to 640 by doubling the resolution in Example 6. The left sub-figure corresponds to the symmetric eigenmode, and the right, the anti-symmetric mode. The colors red, blue, magenta, green, and black correspond to wave numbers  $k_y = 0.5, 1.0, 1.5, 2.0, 2.5$ , respectively. The slopes by the least square fit of these curves are listed in the legend. It shows that the ACIM is about second order. (For interpretation of the references to colour in this figure legend, the reader is referred to the web version of this article.)

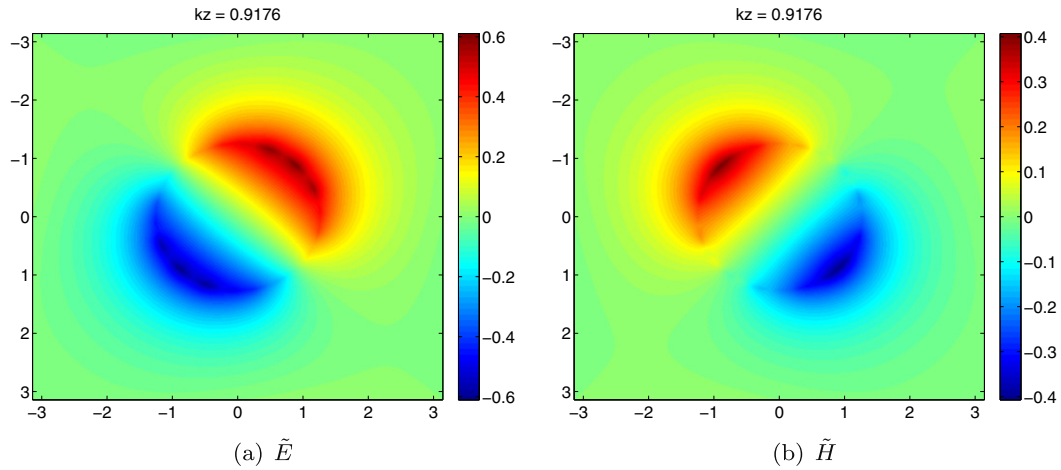


**Fig. 14.** For convergence study in Example 7, we compute a low plasmonic eigenmode in a dielectric hole in metal by ACIM at high resolution ( $N = 640$ ). These sub-figures are its electric and magnetic fields.

We now rotate the coordinate axes by an angle  $\theta$  on the  $y$ - $z$  plane:

$$\begin{pmatrix} x \\ y \\ z \end{pmatrix} = \begin{pmatrix} 1 & 0 & 0 \\ 0 & \cos \theta & -\sin \theta \\ 0 & \sin \theta & \cos \theta \end{pmatrix} \begin{pmatrix} x' \\ y' \\ z' \end{pmatrix}.$$

Then the eigenmode in the new coordinate system is

$$\begin{aligned} \mathbf{E}' &= e^{i(k_x x' + k_z(\sin \theta y' + \cos \theta z') - \omega t)} (0, E_z(x) \sin \theta, E_z(x) \cos \theta) \\ &= e^{i(k_x x' + k_y y' + k_z z') - \omega t} (0, E_y(x), E_z(x)), \\ \mathbf{H}' &= e^{i(k_x x' + k_z(\sin \theta y' + \cos \theta z') - \omega t)} (0, H_y(x) \cos \theta, -H_y(x) \sin \theta) \\ &= e^{i(k_x x' + k_y y' + k_z z') - \omega t} (0, H_{y'}(x), H_{z'}(x)), \end{aligned}$$

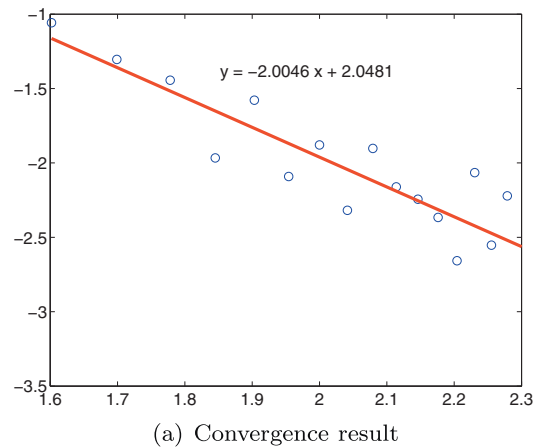


**Fig. 15.** The log-log plot of the error  $|\tilde{k}_{\text{num}}(N) - \tilde{k}_{\text{ref}}|$  of the eigenvalue corresponding to  $\tilde{\omega} = 0.7$  versus  $N$  (the number of intervals in each dimension) for  $N$  ranging from 40 to 200 with  $\Delta N = 10$  in Example 7. The ratio of the radius of the dielectric hole and the length of a unit cell is  $r/a = 0.2$ . The referenced value  $\tilde{k}_{\text{ref}}$  is computed by the same method with  $N = 640$ .

where  $k_y = k_z \sin \theta$ ,  $k_x = k_z \cos \theta$ , and  $k_y^2 + k_x^2 = k_z^2$ . So  $E_z(x', y') = e^{ik_y y'} E_z(x') \cos \theta$  and  $H_z(x', y') = -e^{ik_y y'} H_y(x') \sin \theta$ . We shall use the two dimensional ACIM to compute these non-trivial eigenmodes ( $E_z(x', y')$ ,  $H_z(x', y')$ ). Below, we shall drop the primes for notational simplicity. Fig. 12 shows  $(\tilde{E}, \tilde{H})$  of the symmetric and anti-symmetric with  $\tilde{\omega} = 0.7$ ,  $\tilde{k}_x = 0$ ,  $\tilde{k}_y = 2$  and  $N = 320$ .

To test convergence, we vary  $N$  from 40 to 640 by doubling the resolution. We test with  $\tilde{k}_y = 0.5, 1, 1.5, 2, 2.5$ . Fig. 13 shows the convergence of the corresponding eigenvalue  $\tilde{k}_z$ . It is shown that the convergence of ACIM is second order. Notice that the order of accuracy decreases as  $k_y$  increases because the resolution is not high enough to resolve the thickness of the plasmonic wave, which becomes thinner as  $k_y$  increases.

**Example 7** (Convergence test for plasmonic wave modes in a cylindrical structure). The geometry of our second test problem is a cylindrical dielectric hole sitting in the center of a unit metal cell. In this case, no analytical solution is available. Therefore, for convergence study, we compute a low eigenmode of the surface plasmonic waves for  $\tilde{\omega} = 0.7$  and use a fine grid result ( $640 \times 640$ ) as our referenced solution for comparison. Fig. 14 shows this reference eigenmode. The corresponding eigenvalue is denoted by  $k_{\text{ref}}$ . Then we compute  $k_{\text{num}}(N)$  for  $N$  ranging from 40 to 200 with  $\Delta N = 10$ . Fig. 15 shows the convergence result. The least square fit of the error curve shows that a second order convergence is achieved.

## 5. Concluding remarks

In this paper, we propose an augmented coupling interface method (ACIM) for solving eigenvalue problems with sign-changed coefficients and illustrate its performance by two applications, population dynamics and surface plasmon. The method is formulated on a Cartesian grid by finite difference. The salient features of ACIM include an adaptive-order strategy and an interfacial operator approach coupled with the coupling interface method (CIM) developed previously by the current authors. The adaptive-order strategy of using interpolating polynomials of different orders on different sides of the interfaces avoids the singularity of the local linear system and enables us to handle complex interfaces. The asymptotic analysis suggests that the order should be increased on the side with a larger absolute value of the coefficient. The CIM integrated with the interfacial operators approach further solves the difficulty that jump condition involves the eigenvalues. Numerical validations of convergence are carefully performed. In one dimension, the numerical results show that ACIM with different orders of interpolation near the interface gives second-order and fourth-order convergence of eigenvalues and eigenfunctions. The condition number of the discretization matrix is controlled by the adaptive-order strategy and the accuracy of the eigenvalues is also improved. In two dimensions, due to the lack of the exact solutions in two dimensions, an error estimate is proposed and shows that the method has a second-order accuracy in the sense of global convergence. The method is currently extended to be applicable to the problems in three dimensions. The results will be reported elsewhere.

## Acknowledgements

The work was supported in part by the National Science Council of the Republic of China under Contract Nos. NSC96-2221-E-002-201, NSC97-2628-M-002-020 and NSC97-2115-M-002-004. C.-Y. Kao was partially supported by the U.S. National Science Foundation grant DMS-0811003 and Sloan fellowship. She is grateful to the MBI<sup>f</sup> for the hospitality and support.

## Appendix A. Algorithm

### Algorithm 1. Generalized coupling interface method in one dimension

---

```

1: function (v, d) = CIM1D_GENERAL( $\alpha, a^-, a^+, p, q, r$ )  $\triangleright h = 1$  is assumed
2:  $\mathbf{A} \leftarrow \mathbf{0}_{p+q+2, p+q+2}$ 
3: for  $k \leftarrow 1, p$  do  $\triangleright$  For  $u_{i-p+1:i}$ 
4:    $A_{p+1-k, 1} \leftarrow 1$ 
5:   for  $\ell \leftarrow 1, p$  do
6:      $A_{p+1-k, \ell+1} \leftarrow (k-1)A_{p+1-k, \ell}/\ell$ 
7:   end for
8: end for
9: for  $k \leftarrow 1, q$  do  $\triangleright$  For  $u_{i+1:i+q}$ 
10:   $A_{p+k, p+2} \leftarrow 1$ 
11:  for  $\ell \leftarrow 1, q$  do  $A_{p+k, \ell+p+2} \leftarrow (k-1)A_{p+k, \ell+p+1}/\ell$ 
12:  end for
13: end for
14:  $A_{p+q+1, 1} \leftarrow -1$ 
15: for  $\ell \leftarrow 1, p$  do  $\triangleright [u]$ 
16:   $A_{p+q+1, \ell+1} \leftarrow \alpha A_{p+q+1, \ell}/\ell$ 
17: end for
18:  $A_{p+q+1, p+2} \leftarrow 1$ 
19: for  $\ell \leftarrow 1, q$  do  $[u]$ 
20:   $A_{p+q+1, \ell+p+2} \leftarrow \alpha A_{p+q+1, \ell+p+1}/\ell$ 
21: end for
22:  $A_{p+q+2, 2} \leftarrow -1$ 
23: for  $\ell \leftarrow 1, p-1$  do  $\triangleright [au']$ 
24:   $A_{p+q+2, \ell+2} \leftarrow a^- \alpha A_{p+q+1, \ell+1}/\ell$ 
25: end for
26:  $A_{p+q+2, p+3} \leftarrow 1$ 
27: for  $\ell \leftarrow 1, q-1$  do  $\triangleright [au']$ 
28:   $A_{p+q+2, \ell+p+3} \leftarrow a^+ \alpha A_{p+q+2, \ell+p+2}/\ell$ 
29: end for
30:  $\mathbf{v} \leftarrow \mathbf{0}_{1 \times p+q+2}$   $\triangleright \mathbf{v}$  is a column vector
31:  $v_{1,r} \leftarrow 1$ 
32:  $d \leftarrow \frac{p!q! \det \mathbf{A}}{\min\{|a^-|, |a^+|\}}$   $\triangleright d$  is equal to  $|f_{p,q}(\alpha, \rho)|$ .
33: if  $d \neq 0$  then
34:    $\mathbf{v} \leftarrow \mathbf{v} \mathbf{A}^{-1}$ 
35: end if
36: end function  $\triangleright \frac{d^r u}{dx^r}(x_i) = \frac{1}{h^r} (\sum_{k=1}^{p+q} v_{1,k} u_{i-p+k} + v_{1,p+q+1} [u] + v_{1,p+q+2} h [au'])$ 

```

---

### Algorithm 2. Coupling interface method with adaptive-order strategy in one dimension

---

```

1: function (v, p, q) = CIM1D_GENERAL( $\alpha, a^-, a^+, p, q, r, \epsilon$ )
2: (v, d) = CIM1D_GENERAL( $\alpha, a^-, a^+, p, q, r$ )
3: if  $d < \epsilon$  then  $\triangleright \epsilon$  is the tolerance.
4:   if  $|a^-| > |a^+|$  then  $\triangleright$  adaptive-order strategy in one dimension
5:      $p \leftarrow p + 1$ 
6:   else
7:      $q \leftarrow q + 1$ 
8:   end if
9: end if
10: (v, d) = CIM1D_GENERAL( $\alpha, a^-, a^+, p, q, r$ )
11: end function

```

---

## References

- [1] Z. Li, W. Wang, I. Chern, M. Lai, New formulations for interface problems in polar coordinates, *SIAM Journal on Scientific Computing* 25 (2003) 224–245.
- [2] W. Wang, A jump condition capturing finite difference scheme for elliptic interface problems, *SIAM Journal on Scientific Computing* 25 (2004) 1479–1496.
- [3] Z. Chen, J. Zou, Finite element methods and their convergence for elliptic and parabolic interface problems, *Numerische Mathematik* 79 (1998) 175–202.
- [4] J. Glimm, O. McBryan, A computational model for interfaces, *Advances in Applied Mathematics* 6 (1985) 422–435.
- [5] J. Huang, J. Zou, A mortar element method for elliptic problems with discontinuous coefficients, *IMA Journal of Numerical Analysis* 22 (2002) 549–576.
- [6] Z. Li, T. Lin, X. Wu, New Cartesian grid methods for interface problems using the finite element formulation, *Numerische Mathematik* 96 (2003) 61–98.
- [7] A. Tornberg, B. Engquist, Regularization techniques for numerical approximation of PDEs with singularities, *Journal of Scientific Computing* 19 (2003) 527–552.
- [8] A. Tornberg, B. Engquist, Numerical approximations of singular source terms in differential equations, *Journal of Computational Physics* 200 (2004) 462–488.
- [9] C. Peskin, The immersed boundary method, *Acta Numerica* 11 (2002) 479–517.
- [10] C. Peskin, Numerical analysis of blood-flow in heart, *Journal of Computational Physics* 25 (1977) 220–252.
- [11] R. Leveque, Z. Li, The immersed interface method for elliptic-equations with discontinuous coefficients and singular sources, *SIAM Journal on Numerical Analysis* 31 (1994) 1019–1044.
- [12] Z. Li, K. Ito, Maximum principle preserving schemes for interface problems with discontinuous coefficients, *SIAM Journal on Scientific Computing* 23 (2001) 339–361.
- [13] Z. Li, K. Ito, *The Immersed Interface Method, Numerical Solutions of PDEs Involving Interfaces and Irregular Domains*, SIAM Frontiers in Applied Mathematics, 2006.
- [14] R. Fedkiw, T. Aslam, B. Merriman, S. Osher, A non-oscillatory Eulerian approach to interfaces in multimaterial flows (the ghost fluid method), *Journal of Computational Physics* 152 (1999) 457–492.
- [15] A. Wiegmann, K. Bube, The explicit-jump immersed interface method: finite difference methods for pdes with piecewise smooth solutions, *SIAM Journal on Numerical Analysis* 37 (2000) 827–862.
- [16] P. Berthelsen, A decomposed immersed interface method for variable coefficient elliptic equations with non-smooth and discontinuous solutions, *Journal of Computational Physics* 197 (2004) 364–386.
- [17] Y. Zhou, S. Zhao, M. Feig, G. Wei, High order matched interface and boundary method for elliptic equations with discontinuous coefficients and singular sources, *Journal of Computational Physics* 213 (2006) 1–30.
- [18] I.L. Chern, Y.C. Shu, A coupling interface method for elliptic interface problems, *Journal of Computational Physics* 225 (2007) 2138–2274.
- [19] T. Chen, J. Strain, Piecewise-polynomial discretization and Krylov-accelerated multigrid for elliptic interface problems, *Journal of Computational Physics* 227 (2008) 7503–7542.
- [20] C.C. Chang, R.L. Chern, C.C. Chang, R.R. Hwang, Interfacial operator approach to computing modes of surface plasmon polaritons for periodic structures, *Physical Review B* 72 (2005) 205112.
- [21] F. Belgacem, *Elliptic Boundary Value Problems with Indefinite Weights: Variational Formulations of the Principal Eigenvalue and Applications*, Pitman Research Notes in Mathematics Series, vol. 368, Addison-Wesley-Longman, 1997.
- [22] R.S. Cantrell, C. Cosner, Diffusive logistic equations with indefinite weights: population models in a disrupted environments, *Proceedings of the Royal Society Edinburgh* 112A (1989) 293–318.
- [23] R.S. Cantrell, C. Cosner, The effects of spatial heterogeneity in population dynamics, *Journal of Mathematical Biology* 29 (1991) 315–338.
- [24] Y. Lou, E. Yanagida, Minimization of the principal eigenvalue for an elliptic boundary value problem with indefinite weight and applications to population dynamics, *Japan Journal of Industrial and Applied Mathematics* 23 (2006) 275–292.
- [25] C.Y. Kao, Y. Lou, E. Yanagida, Principal eigenvalue for an elliptic problem with indefinite weight on cylindrical domains, *Mathematical Biosciences and Engineering* (5) (2008) 315–335.
- [26] R.H. Ritchie, Plasma losses by fast electrons in thin films, *Physical Review* 106 (1957) 874–881.
- [27] W.L. Barnes, A. Dereux, T.W. Ebbesen, Surface plasmon subwavelength optics, *Nature* 424 (2003) 824.
- [28] F.I. Baida, A. Belkhir, D.V. Labeke, O. Lamrous, Subwavelength metallic coaxial waveguides in the optical range: role of the plasmonic modes, *Physical Review B* 74 (2006) 205419.
- [29] C.C. Chang, Y.-C. Shu, I.-L. Chern, Solving guided wave modes in plasmonic crystals, *Physical Review B* 78 (2008) 035133.